

## Shallow landslide initiation on terraced slopes: inferences from a physically based approach

Luca Schilirò, Andrea Cevasco, Carlo Esposito & Gabriele Scarascia Mugnozza

To cite this article: Luca Schilirò, Andrea Cevasco, Carlo Esposito & Gabriele Scarascia Mugnozza (2018) Shallow landslide initiation on terraced slopes: inferences from a physically based approach, *Geomatics, Natural Hazards and Risk*, 9:1, 295-324, DOI: [10.1080/19475705.2018.1430066](https://doi.org/10.1080/19475705.2018.1430066)

To link to this article: <https://doi.org/10.1080/19475705.2018.1430066>



© 2018 The Author(s). Published by Informa UK Limited, trading as Taylor & Francis Group.



Published online: 21 Mar 2018.



Submit your article to this journal [↗](#)



Article views: 22



View related articles [↗](#)



View Crossmark data [↗](#)

# Shallow landslide initiation on terraced slopes: inferences from a physically based approach

Luca Schilirò <sup>a</sup>, Andrea Cevasco<sup>b</sup>, Carlo Esposito<sup>a</sup> and Gabriele Scarascia Mugnozza<sup>a</sup>

<sup>a</sup>Department of Earth Sciences, 'Sapienza' University of Rome, Rome, Italy; <sup>b</sup>Department of Earth, Environment and Life Sciences, University of Genova, Genova, Italy

## ABSTRACT

In the last years, great efforts have been made to improve the assessment of the temporal and spatial occurrence of rainfall-induced shallow landslides. Therefore, in this paper we used a physically based stability model (TRIGRS) in order to reproduce the landslide event occurred in the Monterosso catchment (Cinque Terre, Eastern Liguria, Italy) on 25 October 2011. The input parameters of the numerical model have been evaluated taking into account the land-use setting and paying specific attention to the evaluation of the spatial variation of soil thickness on terraced areas. The resulting safety factor maps have been compared with the inventory map of the landslides triggered during the event. The simulation results, which have been obtained also considering four different spatial resolutions of the digital terrain model, emphasize the influence of land use in shallow landslide occurrence and indicate the importance of a realistic spatial variation of soil thickness to enhance the reliability of the model. Finally, different triggering scenarios have been defined using hourly rainfall values statistically derived from historical data. The results indicate the proneness of the area to shallow landsliding, given that rainfall events with a relatively low return period (e.g. 25 years) can trigger numerous slope failures.

## ARTICLE HISTORY

Received 17 May 2017  
Accepted 13 January 2018

## KEYWORDS

Shallow landslides; heavy rainfall; physically based model; terraced slopes; land use

## 1. Introduction

Shallow landslides triggered by rainfall are a widespread hazard that frequently results in considerable damage to infrastructure and human losses in many mountainous regions of the world, especially in areas characterized by the widespread presence of soil cover and subject to heavy precipitation (Aleotti and Chowdhury 1999; Dai et al. 2002; Lin et al. 2006). In order to predict the occurrence of such events, in the last years many attempts have been made to establish a relationship between rainfall and landslides, in particular by means of physically based numerical models. Despite numerous slope stability models have been developed (e.g. Montgomery and Dietrich 1994; Iverson 2000; Borga et al. 2002; Liao et al. 2011; Formetta et al. 2014; Ho and Lee 2016; Thiery et al. 2017), the fundamental controls leading to slope failure driven by rainfall are still not well quantified (Borja et al. 2012), and thus the improvement of current models is still an important research topic (Chang et al. 2008). The difficulty of building up reliable mathematical models lies in the numerous variables involved in the triggering process, such as spatial and temporal rainfall variability, mechanical and hydraulic soil properties, slope morphology, vegetation coverage, initial soil suction and moisture (Greco et al. 2010). However, since it is challenging to comprehensively analyse all these

parameters, it makes sense to focus on those factors that mainly contribute to the onset of the instability. In this respect, land use/land cover is widely considered as a relevant factor for the triggering of shallow landslides (Glade 2003), since it strongly influences different parameters, such as hydrological and mechanical properties of the soil, thickness of the debris cover. Different studies have been performed to evaluate the role of land use in shallow-landsliding, mainly through the use of statistical methods (e.g. Baeza and Corominas 2001; Beguería 2006; Piacentini et al. 2012; Galve et al. 2015; Trigila et al. 2015; Persichillo et al. 2016). These methods are based on conceptual models that describe the functional relationships between instability factors and the past and present distribution of slope failures (Carrara 1983). Bivariate and multivariate approaches are the most common statistical techniques, though probabilistic (e.g. Lee 2005; Goetz et al. 2011, 2015; Youssef et al. 2016; Castro Camilo et al. 2017) and Machine-Learning approaches (e.g. Lee et al. 2004; Ermini et al. 2005; Marjanović et al. 2011; Pham et al. 2017) are also used in this type of analyses. Such approaches are very sensitive to the type and quality of the factors chosen for the susceptibility analysis, and the lack of suitable expert opinion can produce unreliable results (Soeters and Van Westen 1996). Additionally, being data-driven, a statistical model built up for one region cannot readily be extrapolated to the neighbouring area. On the contrary, the main drawback of physically based modeling is the difficulty to gather the input parameters over large and complex areas (Carrara et al. 2008; Chang and Chiang 2009). However, a possible solution is to calibrate the parameter values through back-analysis of preceding major landslide events, after which event-based landslide inventories are generally available (Casadei et al. 2003; Li et al. 2011). In addition, the possibility to consider different triggering inputs makes physically based models particularly suitable for depicting different landslide scenarios, which represents the first step toward a proper hazard analysis.

For these reasons, a well-established model, as TRIGRS (Baum et al. 2008), was used. This model predicts the shallow landslide occurrence by means of the transient, one-dimensional (1D) analytic solution for pore-pressure response to rainfall infiltration with an infinite slope stability calculation (Savage et al. 2003). In particular, the model was applied for the reconstruction via back-analysis of the landslide event occurred on 25 October 2011 in a coastal basin located in Eastern Liguria (Northern Italy), for which a comprehensive event-based landslide inventory has been specifically prepared. For the parameterization of the numerical model, we used a multi-methodological approach recently applied to a similar case study in Southern Italy (Schilirò et al. 2015a, 2015b, 2016); however, we properly modified this approach in order to take into account the specific land-use of the study area, characterized by the widespread presence of agricultural terraces. Specifically, we performed several numerical simulations considering two different methods for the evaluation of the spatial variation of the soil thickness and four different spatial resolutions of the digital terrain model. In addition, since the investigated area has already been affected by flood/landslide events in the past, after evaluating the predictive capability of TRIGRS through comparison with the 2011 landslide inventory we also performed different numerical simulations for depicting future triggering scenarios, on the basis of rainfall values resulting from a statistical analysis of the historical rainfall data.

## 2. The case study

### 2.1. General features of the study area

The study area is located in Eastern Liguria, along the coast of Cinque Terre (Italy) (Figure 1(a)). The Cinque Terre are renowned worldwide as a typical example of man-made landscape, characterized by widespread century-old agricultural terraces retained by dry stone walls. For this reason, this area was declared 'World Heritage Site' by UNESCO in 1997 and successively it was included in the 'Cinque Terre National Park'.

The study area includes six small catchments: namely, Rio delle Rocche, Canale Pastanelli, Fosso Serra, Rio Gaggia, Corone and Fosso Mulinaro. (Figure 1(a)). The wider of these catchments is the

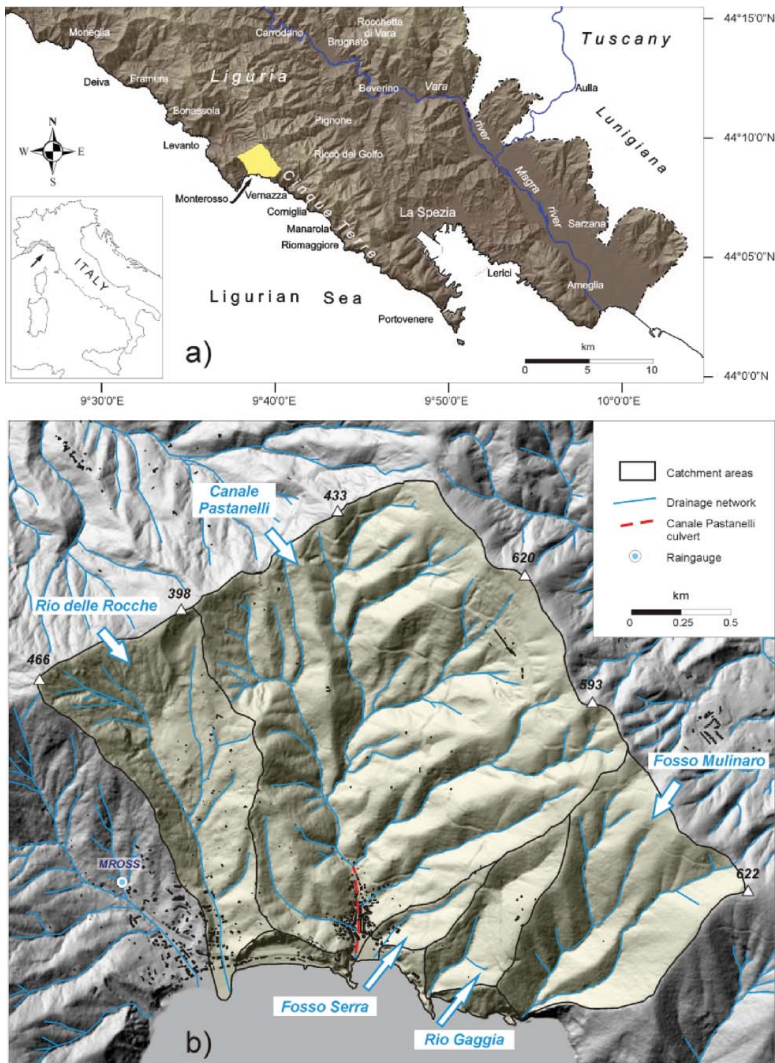


**Figure 1.** (a) Location of the study area and (b) main morphological features of the study area with location of the Monterosso rain gauge (MROSS).

Canale Pastanelli, covering about  $3.2 \text{ km}^2$ . The smallest one, located between the Canale Pastanelli and the Rio Gaggia catchments, is the Fosso Serra, covering about  $0.1 \text{ km}^2$ . The whole investigated area ( $5.4 \text{ km}^2$ ) includes also the Rio delle Rocche, the Rio Gaggia and the Fosso Mulinaro catchments ( $0.95 \text{ km}^2$ ,  $0.27 \text{ km}^2$ , and  $0.86 \text{ km}^2$ , respectively) and some tracts of high rocky coast ( $0.3 \text{ km}^2$ ) (Figure 1(b)).

From a geological point of view (Figure 2(a)), the bedrock is mainly composed of a sandstone-claystone flysch (Riomaggiore Banded Sandstones lithofacies, Macigno Fm., Tuscan Nappe) with rare claystones with limestones and silty sandstones turbiditic rocks (Canetolo Shales and Limestones Fm., Sub-ligurian Domain). Towards W, pelitic rocks (Mt. Veri Shales, External Ligurides), jaspers (Mt. Alpe Jaspers Fm., Internal Ligurides), serpentinites and gabbros (Internal Ligurides) outcrop, respectively (Abbate 1969; Regione Liguria, 2005). On slopes, the sedimentary bedrock is covered by a thin (0.5–2.5 m) eluvial–colluvial soil cover, usually characterized by mixtures of gravel and sand with minor components of silt and clay (Cevasco et al. 2013b, 2014); instead, the ophiolitic

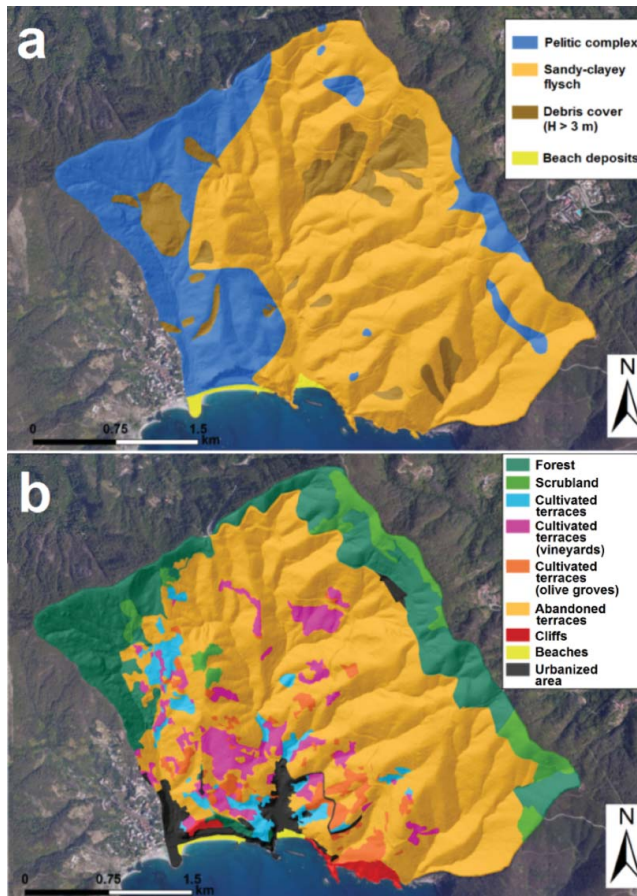


Figure 2. (a) simplified geological map of the Monterosso catchment and (b) land-use map of the Monterosso catchment.

slopes often lack of soil mantle or it is very thin (Cevasco et al. 2015). The shallow soils and debris covers were largely reworked in the past centuries by humans for the building of terraces.

The geomorphological features of the study area, which are controlled by the vicinity of the watershed to the coast, are typical of most coastal basin of the easternmost Liguria. In particular, these catchments have small area (few square kilometres or less than 1 km<sup>2</sup>), high gradient of slopes and short streams with ephemeral hydrological regime. More than 40% of the slope angles are ranging between 30° and 40°. The characteristics above, along with the urbanization of the Monterosso village, which mainly developed on the floor of the Rio delle Rocche and Canale Pastanelli valleys, make Monterosso particularly exposed to flood risk. In addition, the conditions imposed by the coverage of the final tracts of both the Rio delle Rocche and Canale Pastanelli, for about 400 m upstream of the marina, increase the risk of flooding (Figure 1(b)). Peculiar land-use features, typical in Cinque Terre and Liguria, characterize the study area. Despite the slopes were almost completely terraced during the past centuries (about 71% of the study area) for vineyards and oliveyards, only 19% of the total terraced areas (about 14% of the study area) is still cultivated (Figure 2(b)). A very similar ratio between cultivated terraces vs. total terraced area characterizes the Vernazza catchment (Cevasco et al. 2013a), close to the study area (Figure 3). This point indicates how the social changes occurred in the second half of 1950s affected the land use at Cinque Terre. On abandoned terraced areas, vegetation spreads quite rapidly. At first, a vegetation consisting mainly of scrubs grows up



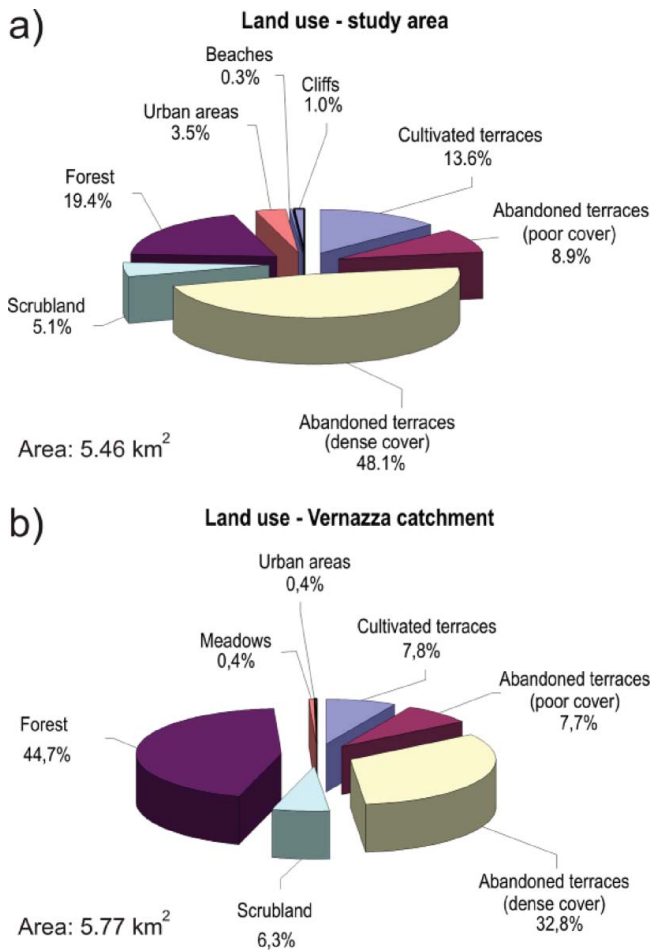


Figure 3. (a) Land-use study area and (b) Vernazza catchment in 2011 (Cevasco et al. 2014).

sparingly. After a time span of about 25-30 years, a dense vegetation constituted by forest tree species (mainly pine, mixed woods, chestnut woods, holm oak woods) or by Mediterranean scrub covers abandoned terraces (Brandolini et al. 2016).

The climate of the study area is Mediterranean, particularly mild due to geographical and morphological peculiarities. In general, summers are hot and dry, winters are mild and autumn is the rainiest season. Based on the analysis of 1954–2012 data from the Levanto rain gauge (4 km NW from the study area), the mean annual precipitation is 1033 mm, whereas the rainiest month is October, with a mean precipitation of 154 mm (Cevasco et al. 2015). The mean annual precipitation tends to increase with altitude moving from the coast to the watershed (Pedemonte 2005). In particular, in the proximity of the culminations of the watershed bounding the study area to the N the mean annual precipitation reaches about 1200 mm.

Due to self-regenerating storm cells or to persistent cyclonic Tyrrhenian circulation (Crosta 1998; Cevasco et al. 2009), extreme precipitation can occur, between late summer and mid-autumn, along the coast of eastern Liguria (van Delden 2001; Silvestro et al. 2012, 2015; Rebori et al. 2013; Buzzi et al. 2014; Cevasco et al. 2015; Cassola et al. 2016). Usually these rainstorms have short duration (<24 h), but rainfall intensities can reach or exceed values of 100 mm h<sup>-1</sup>.

## 2.2. The 25th October 2011 event and previous flooding events

On 25 October 2011 extreme precipitation hit a wide area between east Liguria and north-west Tuscany. In particular, a violent storm system with a ‘self-healing’ structure originated over the Cinque Terre area in very short time, caused extreme rainfall between 7:00 and 17:00 (Universal Time Coordinated, UTC) along the coast and the inland Vara valley (east Liguria), and then it moved to the Lunigiana (north-western Tuscany). Based on data from Regione Liguria (2012), at the Monterosso rain gauge a cumulative rainfall of 382 mm was recorded, with maximum rainfall intensities reaching 90 mm/h, 195 mm/3 h and 350 mm/6 h (Figure 4). Higher values, regarding both the cumulative rainfall and the rainfall intensities, were recorded at the Brugnato rain gauge (Vara valley, about 10 km NE from the study area), with cumulative rainfall of 538 mm and maximum rainfall intensities reaching 153 mm/h, 328 mm/3 h and 472 mm/12 h, respectively. Hundreds of shallow landslides and floods affected the Tyrrhenian coastal basins between Bonassola and Manarola and the Magra river basin (Cevasco et al. 2012, 2013a; D’Amato Avanzi et al. 2013, 2015), causing 13 casualties and very severe damage to villages and infrastructures. In the study area, the Monterosso village was affected by a catastrophic mud/debris flood. Enormous amount of earth and debris, mobilized on slopes and charged by torrents downhill, overwhelmed the central streets of Monterosso as consequence of the filling of the final culvert of the Canale Pastanelli. The maximum thickness of deposited materials reached about 3 m in the centre of the village. One casualty occurred and shops and restaurants were devastated.

After the 25th October 2011 rainstorm, a detailed rainfall-induced landslide inventory was specifically compiled for the study area through analysis of high-resolution aerial photographs and field surveys. The air photo analysis was carried out on digital geo-referenced orthophotos, provided by Liguria Regional Administration, taken on 11 November 2011 by the Air Service of Remote Sensing and Monitoring of Civil Protection of Friuli Venezia Giulia Regional Administration (ground

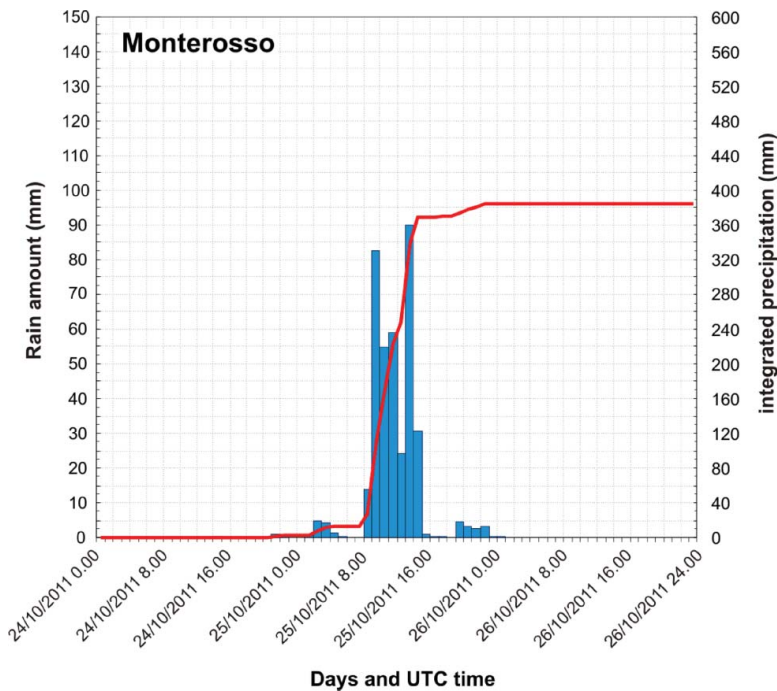


Figure 4. Hyetograph (blue bar) and cumulative rainfall plot (red line) between 00.00 UTC of the 24th October 2011 and 24.00 UTC of the 26th October 2011 of the Monterosso rain gauge (data from Regione Liguria 2012).

resolution from 3 to 50 cm, according to the altitude). The high resolution of aerial photographs allowed to achieve great detail in the mapping of landslides.

A total of 260 shallow landslides were mapped in the study area, more than 214 of which occurred in the Rio delle Rocche and the Canale Pastanelli catchments. The shallow landslides triggered on 25 October 2011 initiated as debris slides (Cruden and Varnes 1996) and in most of cases evolved into debris avalanches or, in few cases, into debris flows (Hungri et al. 2014). Shallow earth and debris covers (from 0.5 m to about 2.5 m thick) and, sometimes, portions of the weathered and fractured bedrock were involved. According to the landslide classification by Hungri et al. (2014), we considered as debris avalanches 'very rapid shallow flows of partially or fully saturated debris on a steep slope, without confinement in an established channel' and as debris flows 'very rapid to extremely rapid flow of saturated non-plastic debris in a steep channel'. The total area affected by landslides was about 6.5 ha, corresponding to 1.2% of the study area, whereas the average density of landslides was 47.6 landslides/km<sup>2</sup>. Landslide areal extent ranged between few tens of square metres up to few thousands square metres. Earth and debris mobilized on slopes or along channels by shallow landslides increased the sediment transport along the drainage network and also the erosive energy of streams. The inability to dispose flowing of water/sediment mixtures of the final culvert of the Canale Pastanelli, played a fundamental role in originating the mud/debris flood that affected the Monterosso village.

However, in the last century, another disastrous flood occurred on 2 October 1966 at Monterosso. Data about this event were collected on the 'Italian archive of historical information on landslides and floods' (Guzzetti et al. 1994; Guzzetti and Tonelli 2004), Italian newspapers and local chronicles. The flood occurred in the evening of the 2 October 1966. The central streets of Monterosso were flooded by water and earth, spreading on basements, shops, bars and sweeping away towards the sea the boats standing on the beach. Newspapers reported images showing the central street of the village (Figure 5(a)), as well as the area between the railway and the marina, flooded by water and debris. From the comparison of these images with those depicting the same areas after the 25 October 2011 flood one can deduce that the effects of the two floods were of comparable size (Figure 5(b)). Another sign testifying the similarity between the effects of these two floods was imprinted on the wall of the S. Giovanni Battista Church, located just upstream the marina, indicating the maximum level (about 2.5 m) reached by water and debris in both floods (Figure 5(c)).

The flood event occurred in 1966 caused severe damage to people, buildings and infrastructures. In particular, 50 displaced persons and 300 homeless were estimated (AVI database, <http://sici.irpi.cnr.it/>). The same database reports that rainfall lasted 14 h continuously. Since no rainfall data for that event were available for the Monterosso rain gauge, we referred to the nearest Levanto rain gauge. The rainfall started on 30 September 1966 and lasted until 4 October 1966. A total rainfall of 263 mm was recorded in these five days but 142 mm were recorded just from 2 October 1966 to 3 October 1966. Maximum intensity rainfall of 85 mm/6 h, 127 mm/12 h and 152 mm/24 h were recorded during that event. By comparing rainfall data of 1966 and 2011 floods, it results that the 2011 event was the most severe.

### 3. Methodology

The work described in this paper can be divided in three stages. First, we performed a back-analysis of the 25 October 2011 event by comparing the resulting triggering scenarios with the inventory of the landslides occurred during the event. Afterwards, we performed a statistical analysis of the historical rainfall data available for the study area in order to evaluate the recurrence of specific rainfall events. Finally, once the physically based model was validated through the back analysis of the reference landslide event, we reconstructed different triggering scenarios by using rainfall inputs, whose return periods (RPs) have been defined through the preceding statistical analysis.





**Figure 5.** (a) the central way of Monterosso flooded on 2 October 1966 (La Stampa 1966) and (b) on 25 October 2011 (photo A. Cevasco); (c) maximum levels reached by floods on 2 October 1966 and on 25 October 2011 imprinted on the wall of the S. Giovanni Battista church at Monterosso (photo A. Cevasco).

### 3.1. Theoretical basis of TRIGRS model

TRIGRS (Transient Rainfall Infiltration and Grid-based Slope Stability model) is a physically based model devoted to the spatial and temporal prediction of rainfall-induced shallow landslides over large areas. The model performs an infinite-slope stability calculation accounting for the pressure head response  $\Psi(Z,t)$  to a time-varying rainfall input on the ground surface  $I_Z(t)$ . Specifically, the infiltration process is simulated considering the 1D analytic solution of Richards' equation as well as described by Iverson (2000). In the most recent version of the program (Baum et al. 2008), TRIGRS was expanded to address infiltration also into unsaturated soils, then assuming a two-layer system consisting of a saturated zone (with the possible presence of a capillary fringe) and an unsaturated zone that extends to the ground surface (Figure 6). For the linearization of Richards' equation within the unsaturated zone, TRIGRS considers the Gardner (1958) hydraulic model, which is based on the definition of four main hydrodynamic parameters: the saturated ( $\theta_s$ ) and residual ( $\theta_r$ ) water content, the saturated hydraulic conductivity ( $K_s$ ) and a specific parameter linked to the pore size distribution ( $\alpha_G$ ). According to the hydraulic model, the unsaturated zone absorbs part of the water that infiltrates through the ground surface, while the remaining water accumulates above the initial water table. If the amount of infiltrated water exceeds the maximum amount that can be drained by gravity, TRIGRS simulates the water-table rise comparing the exceeding water quantity to the available pore space directly above the water table or capillary fringe. On the basis of the new water table level, the model then computes the new pressure head value (Baum et al. 2010). Finally, the Safety Factor at depth  $Z$  is calculated on the basis of a series of input parameters locally

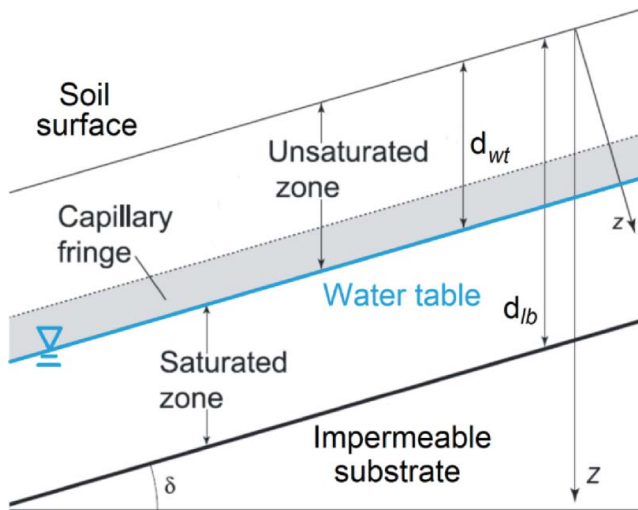


Figure 6. Conceptual sketch of the hydrological model in TRIGRS (modified from Baum et al. 2010).

variable throughout the model:

$$FS(Z, t) = \frac{\tan\phi'}{\tan\delta} + \frac{c' - \psi(Z, t)\gamma_w \tan\phi'}{\gamma Z \sin\delta \cos\delta} \quad (1)$$

where  $\delta$  is the slope angle,  $c'$  is the soil-cohesion for effective stress,  $\phi'$  is the soil friction angle for effective stress,  $\gamma_w$  is the unit weight of groundwater and  $\gamma$  is the total unit weight of soil.

### 3.2. Evaluation of TRIGRS input parameters and assumptions in the light of a preceding case study

In view of back-analysing the 25 October 2011 event, we evaluated the input parameters of TRIGRS through an approach based on the application of different methods and techniques. This approach has been already tested (Schilirò et al. 2015a; 2016) in a similar case study occurred in Southern Italy on 1 October 2009. On that day, a heavy rainstorm triggered several hundreds of shallow landslides in the southern Messina area (north-eastern Sicily), causing 37 fatalities and severe damage to buildings and infrastructure, mostly near the village of Giampileri (Schilirò and Esposito 2013). The choice of using the same approach can be then explained considering the similarities between the two case studies. In fact, the geological and geomorphological contexts are very similar given the presence, in both areas, of a thin eluvial–colluvial soil cover above an impermeable bedrock and of small coastal basins having steep slopes with torrent-like straight watercourses. Furthermore, the triggering events are comparable to each other, being both related to a violent storm system with a ‘self-healing’ structure which caused extreme, short duration rainfall events with extremely high intensity peaks. The typology of triggered landslides is substantially the same (Figure 7) and probably reflects similar triggering conditions, also considering the similarities between the involved materials, both characterized by high content of coarse grained particles with minor components of silt and clay (Table 1). Precisely in order to investigate the failure mechanisms of the soil cover in a wide range of initial conditions (i.e. porosity and water content), in a recent study (Montrasio et al. 2016) specific laboratory flume tests have been conducted on the material sampled near Giampileri, and the development of the failure process was also numerically simulated with SLIP, a simple physically based model that predicts the triggering of shallow landslides on the basis of the soil

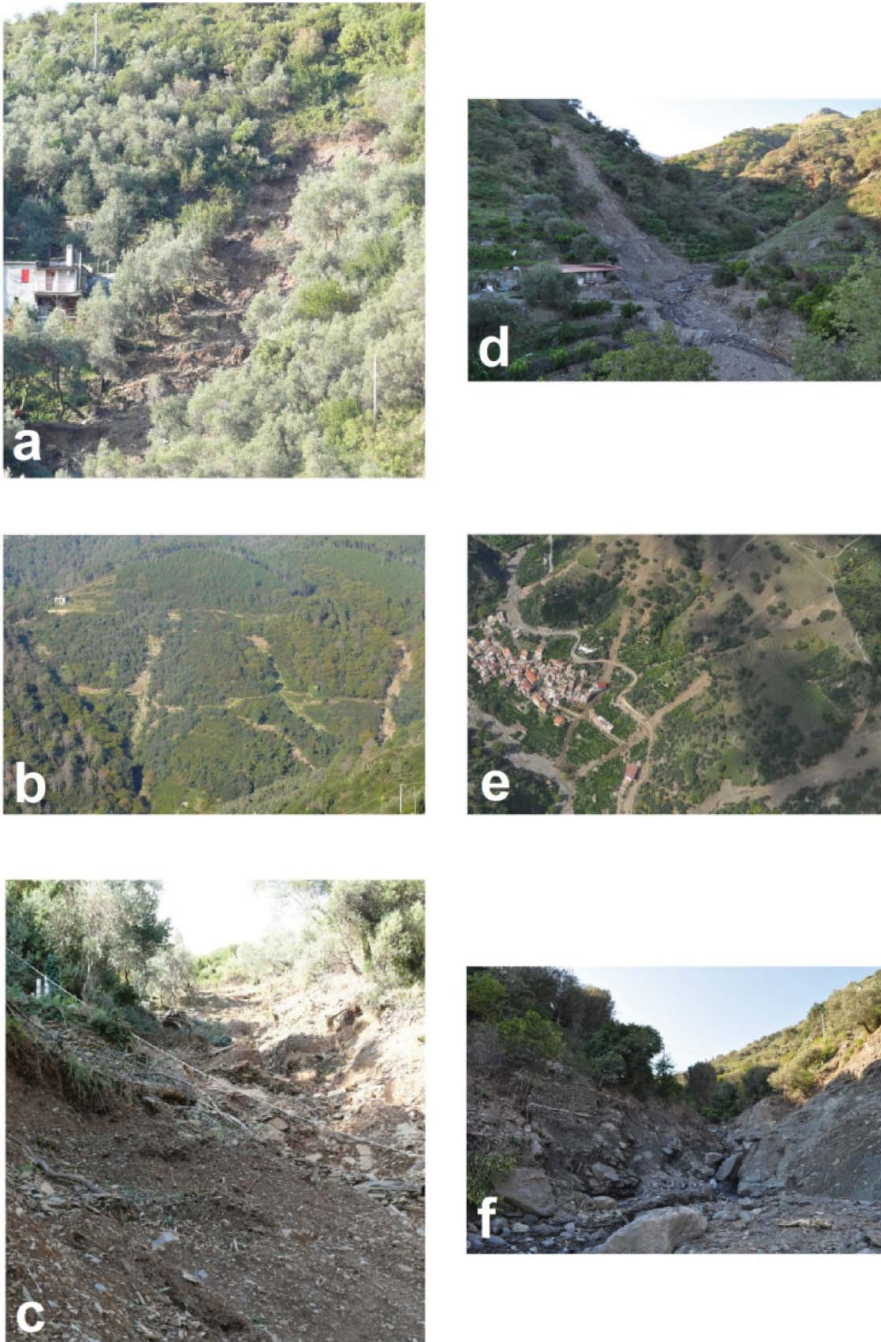


**Figure 7.** Examples of shallow landslides occurred in the Monterosso catchment on 25 October 2011; (a, b) and in Giampilieri village (Messina, north-eastern Sicily, Southern Italy) during the 1st October 2009 event (d, e). Figure c and f show the features of the shallow covers after the triggering of the landslides in Monterosso and Giampilieri, respectively.

**Table 1.** Average granulometric characteristics of the colluvial deposits outcropping in the Monterosso catchment and on the slopes near Giampilieri.

	<i>Monterosso</i>	<i>Giampilieri</i>
Gravel (%)	52.5	58.1
Sand (%)	26.5	30.6
Silt (%)	16	9.5
Clay (%)	5	1.8





Figure 8. Post-failure images of flume tests performed on the material sampled near Giampilieri (from Montrasio et al. 2016 mod.)

characteristics and the rainfall amount (Montrasio 2000; Montrasio and Valentino 2008). The results of the experimental tests substantially agree with the outcome of the numerical simulations, since the mean variation between real and predicted failure time is in the order of a few minutes, even for the longest tests (Montrasio et al. 2016). Furthermore, it is interesting to note that not only the shallowest part, but also the inner part of the soil profile appeared saturated after the failure (Figure 8). This feature fits with the hydrological model implemented in SLIP, which assumes a water flow through the soil macropores that generates a progressively saturation of non-adjacent volumes of soil (Zhang and Zhang 2009): if the raining process persists, the saturated portions of soil extend and become continuous (Figure 9) and the sliding process starts when a relatively wide continuous stratum of saturated soil has formed. Although no measurements of pore water pressure have been recorded during these tests, in previous works (i.e. Montrasio and Valentino 2007, 2008), experimental measurements of suction and pore pressure have been recorded during flume tests under different rainy conditions, confirming that shallow soil layers reach a zero value of suction well before the deeper ones and the first slip occurs only after the matric suction has dropped to zero everywhere. This condition corresponds to a state of complete saturation of the soil layer that is in contact with the impermeable bed (Montrasio and Valentino 2007). The reliability of the SLIP model was also substantiated by the results obtained for the back-analysis of the 2009 event at the catchment scale (Schilirò et al. 2016). In this respect, it is worth noting that these results are similar to those obtained with TRIGRS: this point suggests the similarities between the two models, despite a different way to simulate the infiltration process. However, it is important to stress that SLIP bypasses the transient analysis of the infiltration process assuming the formation, as a consequence of a rainfall event, of the final condition of a perched water table akin to that resulting from the TRIGRS simulations.

Therefore, on the basis of the remarks pointed out above, we have defined the TRIGRS input parameters (Table 2) by using different types of data available for the Monterosso area. A detailed

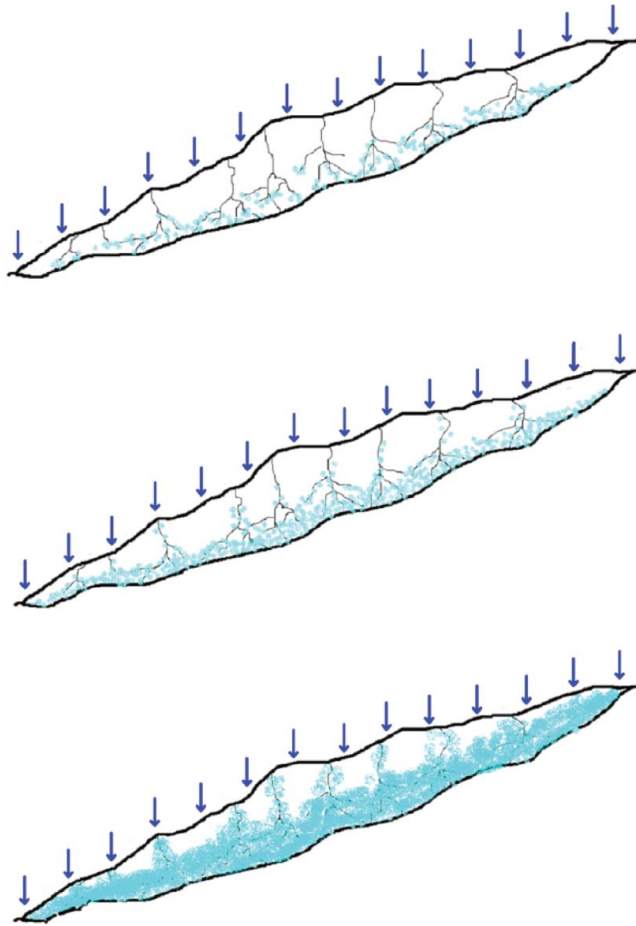


Figure 9. From top to bottom: evolution of saturation process through the soil macropores (from Montrasio and Valentino 2008)

( $1 \times 1$  m) pre-event digital elevation model (DEM), deriving from airborne LiDAR data, has been used as basic information for the numerical simulations. The original DEM has also been resampled to 2, 4 and 8 meters by using the bi-cubic polynomial interpolation technique, with the aim of evaluating the simulation results at different resolutions. Accurate geological and land-use maps (Figure 2), resulting from air photo analysis, field surveys and site investigations, have been used for the evaluation of the spatial variation of some specific parameters. For instance, the estimation of soil thickness (Figure 10) has been performed by correlating soil depth to the local slope angle (Saulnier et al. 1997):

$$h_i = h_{\max} \left\{ 1 - \left[ \frac{\tan\alpha_i - \tan\alpha_{\min}}{\tan\alpha_{\max} - \tan\alpha_{\min}} \left( 1 - \frac{h_{\min}}{h_{\max}} \right) \right] \right\} \quad (2)$$

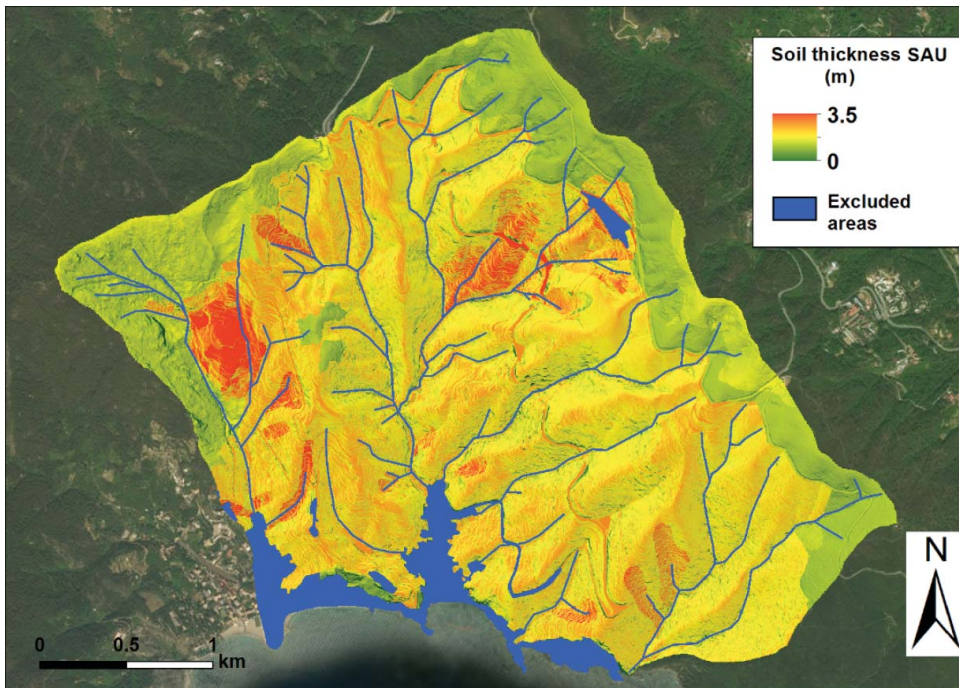
where  $h_i$  and  $\alpha_i$  are, respectively, the soil thickness and the slope measured at pixel  $i$ , whereas  $h_{\max}$ ,  $h_{\min}$ ,  $\alpha_{\max}$  and  $\alpha_{\min}$  are the maximum and minimum thickness-slope values encountered in each terrain unit, identified from the overlap of the geological and land-use maps (Figure 11). The soil thickness ranges have been defined according to field measurements performed in the neighbouring Vernazza basin (Cevasco et al. 2013b, 2014), since this basin has quite similar geological and geomorphological features to the study area. However, the spatial variation of the soil thickness can be



**Table 2.** Input parameters for the TRIGRS model.

Parameter		Attributed value	Source
$\delta$ (°)	Slope	Spatial map	1 × 1 m DEM
$H$ (m)	Soil thickness	Spatial map	Saulnier et al. (1997)
$d_{wt}$ (m)	Initial water table depth	H	Topographic Position Index
$I_{ZLT}$ (m s <sup>-1</sup> )	Background rainfall rate	$1.09 \times 10^{-8}$	HYDRUS 1D
$\theta_s$ (-)	Saturated water content	0.3815	HYDRUS 1D
$\theta_r$ (-)	Residual water content	0.0485	HYDRUS 1D
$K_s$ (m s <sup>-1</sup> )	Saturated hydraulic conductivity	$4.63 \times 10^{-6}$	HYDRUS 1D + calibration
		$2.55 \times 10^{-5}$ (long-time abandoned terraces)	
		$4.63 \times 10^{-5}$ (forest-scrubland)	
$D_0$ (m <sup>2</sup> s <sup>-1</sup> )	Hydraulic diffusivity	$2.39 \times 10^{-5}$	Johnson (1967)
		$1.32 \times 10^{-4}$ (long-time abandoned terraces)	
		$2.39 \times 10^{-4}$ (forest-scrubland)	
$\alpha_G$ (m <sup>-1</sup> )	Gardner parameter	18.3	HYDRUS 1D + Ghezzehei et al. (2007)
$\varphi'$ (°)	Friction angle	31	Cevasco et al. (2014)
$c'$ (kN m <sup>-2</sup> )	Cohesion	5.0	Calibration
		4.5 (recently abandoned terraces)	
		5.5 (long-time abandoned terraces)	
		6.0 (forest-scrubland)	
$\gamma_n$ (kN m <sup>-3</sup> )	Soil unit weight	16.33	Cevasco et al. (2014)
$I_z$ (m s <sup>-1</sup> )	Rainfall rate	Spatial-temporal maps	ARPAL Agency

highly influenced by the widespread presence of agricultural terraces, which represent one of the most relevant peculiarities of the Cinque Terre area. For this reason, we performed an alternative soil thickness estimation by using a morphometric approach. Since the available DTM is enough detailed to reproduce the morphological variations due to agricultural terraces, the basic idea was to


**Figure 10.** 1-m soil thickness map according to the Saulnier's method.

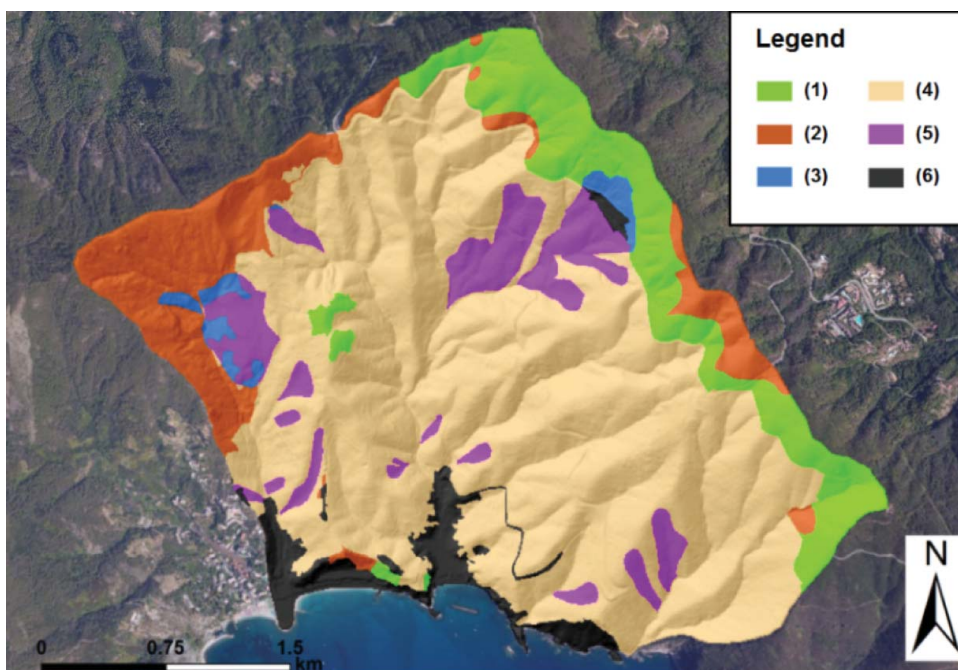


**Figure 11.** Terrain units defined by combining the geological and land-use maps (see Figure 2): 1 – forest and scrubland on flysch ( $H = 0.5\text{--}1.3$  m), 2 – forest and scrubland on pelitic complex ( $H = 0.5\text{--}1.6$  m), 3 – forest and scrubland on debris cover ( $H = 0.5\text{--}3$  m), 4 – Terraces, olive groves and vineyards ( $H = 0.5\text{--}2.5$  m), 5 – Terraces, olive groves and vineyards on debris cover ( $H = 0.5\text{--}3.5$  m), 6 – Cliffs, beaches and urbanized area ( $H = 0$  m).

analyse the stepped slope morphology by means of quantitative morphometric indexes to account for the ‘cyclic’ soil thickness variation that occurs moving from the downslope-facing wall of a terrace (maximum thickness) to the innermost part of the flat slope (minimum thickness) featuring the proper terrace. For this purpose, the Topographic Position Index (TPI) algorithm (Weiss 2001) has been tested to analyse the terrain morphology at a very low wavelength, with the final aim of zoning the terraced areas in terms of soil thickness. The TPI algorithm performs an automated land-form classification by comparing the elevation of each DTM cell with the surrounding ones. The resulting values are strongly dependent on the size of the considered neighbourhood and the shape of the search window. Starting from the TPI values, it is possible to partition the territory according to the Slope Position Index (SPI), which provides for the classification of the TPI continuous values according to specific threshold values that are based on the standard deviations of TPI. Assigning a SPI value to each cell allows to define its relative position with respect to the topographic structure, i.e. – for example – whether a DTM cell element belongs to a flat area, or represents a portion of a ridge, a valley or a slope (low, middle and upper). For this case study, after several attempts to find the ‘best fit’ search window in terms of both radius and shape, it was possible to select a circular window with a 6 m radius. The results have been validated by comparison with the actual topography. Furthermore, after having classified the TPI values in terms of SPI, it was possible to partition the terraced slopes in zones (namely ‘valleys’, ‘lower slope’, ‘mid slope’, ‘upper slope’, ‘ridge’ and ‘flat slope’) (Figure 12) having different average soil thicknesses. The values of soil thickness related to each SPI class have been estimated based on the knowledge of the technique used to build the agricultural terraces. The resulting map is represented in Figure 13: however, it is important to note that we used the TPI method for the terraced areas only, while we continued to employ the Saulnier’s method for those not terraced, assuming that these areas are not influenced by human actions and the soil thickness then depends on the natural slope conditions. In addition, since TRIGRS is

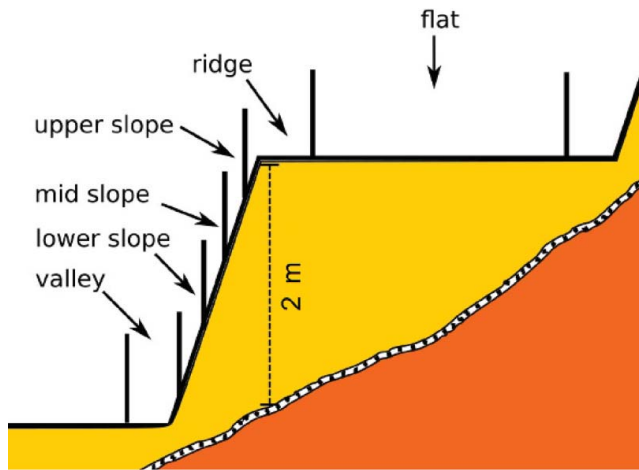


**Figure 12.** Simplified sketch of the TPI-based classification of terraced slopes. Each SPI class is characterized by an average soil thickness (namely, valley = 0.2 m, lower slope = 0.5 m, mid slope = 1 m, upper slope = 1.5 m, ridge = 2 m, flat = 1.2 m). On the areas characterize by the presence of thick debris covers (see Figure 2(a)), the average thickness values have been consistently increased (namely, valley = 1 m, lower slope = 1.5 m, mid slope = 2 m, upper slope = 3 m, ridge = 3.5 m, flat = 2.5 m).

specifically aimed at the analysis of shallow landslide initiation on slopes, the beaches and the urbanized areas, as well as the gullies and the cliffs, have been excluded from the thickness calculation both with the TPI and the Saulnier's method.

An evaluation of the consistency of the two resulting soil thickness maps has been also made by using a  $1 \times 1$  m post-event DEM, which is likewise available for the study area. In detail, we compared the pre- and post-event DEMs in order to calculate the elevation difference into the landslide

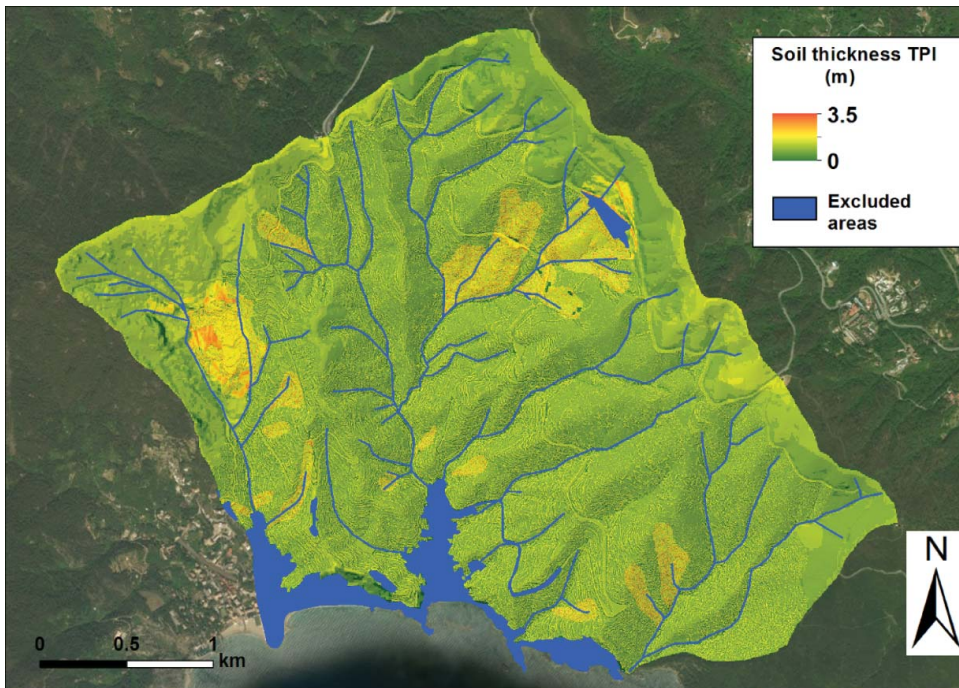


**Figure 13.** 1-m soil thickness map according to the Topographic Position Index method.



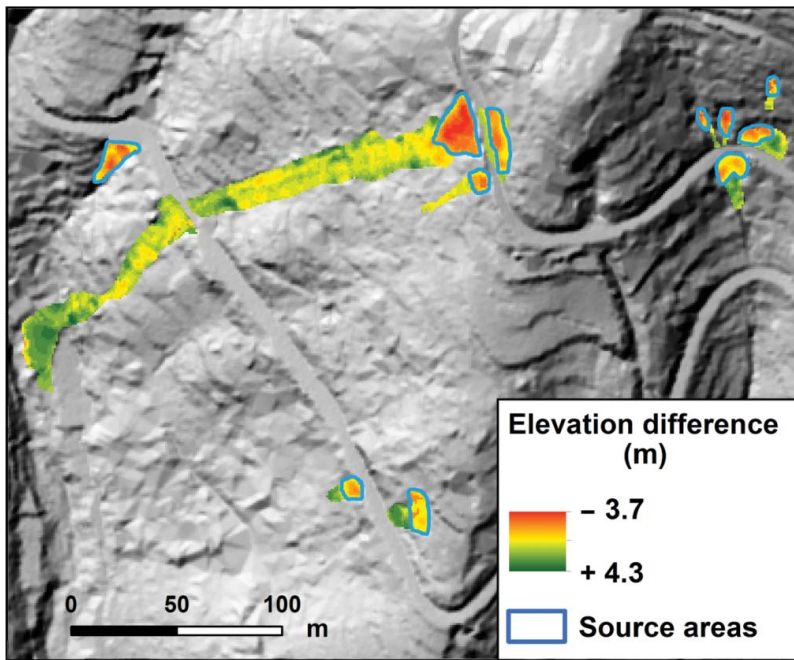


Figure 14. Pre- and post-event digital elevation models (DEMs) illustrating the elevation differences within the landslide areas after the 25th October 2011 event.

areas (Figure 14). In this respect, it is important to note that for each mapped landslide the deposit has been distinguished from the source area through the analysis of high-resolution aerial orthophotos, integrated by field surveys in the days after the event. At this point, we can assume that the elevation difference calculated within only the source areas coincides with the actual soil thickness, considering that in numerous cases the bedrock was exposed after the landslide occurrence.

Therefore, we compared the average elevation difference calculated for each of 260 source areas with the corresponding average soil thickness value estimated with the TPI and Saulnier's method at different spatial resolutions. The results, that have been expressed in terms of Mean Absolute and Root Mean Square Error (Table 3), indicate that the mean error is always higher (+ 20–30 cm) in the case of maps obtained by using the Saulnier's method. The difference between the two methods is very low just with the 8-m resolution, probably due to the excessive coarseness that does not allow to correctly reproduce the terraces' spatial pattern. However, it is important to stress that estimating the spatial variation of the soil thickness at the catchment scale can be difficult and often unreliable, since this parameter is strongly influenced by different interplaying factors, such as underlying lithology and vegetation cover (Catani et al. 2010). For this reason, an MAE ranging between 0.49 and 0.67 m (for the soil thickness map obtained with the TPI method) can, however, be considered a reasonably good result, especially in relation to the complexity of the territorial context typical of

Table 3. Mean absolute (MAE) and root mean square (RMSE) Errors obtained from the comparison, at different spatial resolutions, between the average elevation differences calculated for each mapped source areas and the corresponding average soil thickness values estimated with the TPI and Saulnier's method.

Spatial resolution	Topographic Position Index		Saulnier's method	
	MAE (m)	RMSE (m)	MAE (m)	RMSE (m)
1 m	0.49	0.64	0.72	0.88
2 m	0.50	0.66	0.75	0.96
4 m	0.53	0.68	0.78	0.98
8 m	0.67	0.87	0.70	0.85

**Table 4.** Mean absolute (MAE) and root mean square (RMSE) errors obtained from the comparison, at different spatial resolutions, between the average elevation differences calculated for each mapped source areas and the corresponding average soil thickness values estimated with the TPI and Saulnier's method. In this case, the analysis has been performed for six different zones, identified on the basis of the agricultural terrace type (i.e. still cultivated, recently-abandoned or long-time abandoned terrace) and the presence-absence of underlying thick debris covers.

Zone	Spatial resolution	MAE (m)		RMSE (m)		Zone	Spatial resolution	MAE (m)		RMSE (m)	
		TPI	SAU	TPI	SAU			TPI	SAU	TPI	SAU
Cultivated terraces on debris cover	1 m	0.85	1.18	0.95	1.30	Cultivated terraces	1 m	0.42	0.81	0.52	0.94
	2 m	0.83	1.04	0.87	1.61		2 m	0.46	0.72	0.31	0.88
	4 m	0.49	0.86	0.32	0.98		4 m	0.49	0.57	0.46	0.55
	8 m	0.79	0.81	0.84	0.71		8 m	0.44	0.62	0.30	0.58
Long-time abandoned terraces on debris cover	1 m	0.67	1.18	0.75	1.28	Long-time abandoned terraces	1 m	0.45	0.58	0.56	0.70
	2 m	0.72	1.02	0.67	1.70		2 m	0.47	0.74	0.34	0.86
	4 m	0.61	1.00	0.56	1.50		4 m	0.50	0.50	0.44	0.42
	8 m	0.51	0.75	0.43	0.88		8 m	0.62	0.59	0.72	0.59
Recently abandoned terraces on debris cover	1 m	0.90	1.01	1.00	1.15	Recently abandoned terraces	1 m	0.39	0.56	0.52	0.70
	2 m	0.92	0.90	1.09	1.01		2 m	0.37	0.61	0.29	0.63
	4 m	0.75	1.04	0.68	1.30		4 m	0.40	0.50	0.33	0.41
	8 m	1.00	1.39	1.03	2.16		8 m	0.53	0.69	0.60	0.69

the Cinque Terre area. In this sense, we performed a further analysis in order to describe the variation of MAE and RMSE as a function of the agricultural terrace type (i.e. still cultivated, recently-abandoned or long-time abandoned terrace) and the presence-absence of underlying thick debris covers. The first distinction has been made for taking into account the potential influence of the vegetation cover on the estimation of the soil thickness, considering that the vegetation is much sparse in the case of still cultivated and recently abandoned terraces. According to the results (Table 4), the highest errors have been obtained for the areas characterized by the presence of thick debris covers, where the difference between estimated and real soil thickness is generally higher than 70 cm. On the contrary, such difference can be also lower than 40 cm for the terraced areas where the underlying debris cover is absent. However, it is important to note that the error calculated for the areas where the debris cover is present may be affected by the fact that in different landslide detachment zones the sliding surface did not develop at the contact with the underlying bedrock, but within the soil profile. Therefore, in such areas the real soil thickness can be underestimated, and the comparison with the value estimated with the TPI and Saulnier's method may be not completely truthful. Nonetheless, also in this analysis the mean error is always higher for the maps obtained with the Saulnier's method, whereas there does not seem to be any particular influence of the vegetation cover, considering that there is not any remarkable difference of the MAE and RMSE by varying the terrace type, both in the presence and absence of the underlying debris cover.

For the estimation of the initial soil moisture conditions during the 25 October 2011 event, we employed the same approach used in the Giampilieri study case (Schilirò et al. 2015a): therefore, we considered the 1-month antecedent rainfall fallen in the study area by using the HYDRUS 1D model (Šimůnek et al. 1998), which can simulate the water flow into unsaturated porous media resulting from a rainfall event. Daily rainfall data have been used as input for the model, whereas evapotranspiration is accounted for by inserting the maximum and minimum temperature values recorded during the investigated period into the Hargreaves equation (Jensen et al. 1997). As a lower boundary, a zero-flux condition was assumed due to the presence of impermeable bedrock below the soil cover. A 1.5 m soil profile inclined to 30° (i.e. the average soil thickness and slope observed within the landslide source areas) was chosen as the most representative geometric configuration of the slope prior to the 2011 event. Therefore, a differentiation between terraced and not terraced areas was not made since just very few source areas are located in not terraced areas; however, it is important to stress that these areas represent just a limited portion of the entire study area compared with that covered by agricultural terraces (i.e. 24% vs. 71%, see Figure 3(a)). The initial soil moisture was assumed to be near to the residual water content value ( $\theta_r$ ) considering the hot, dry conditions during the preceding summer months. In fact, HYDRUS 1D has been also used not only for predicting



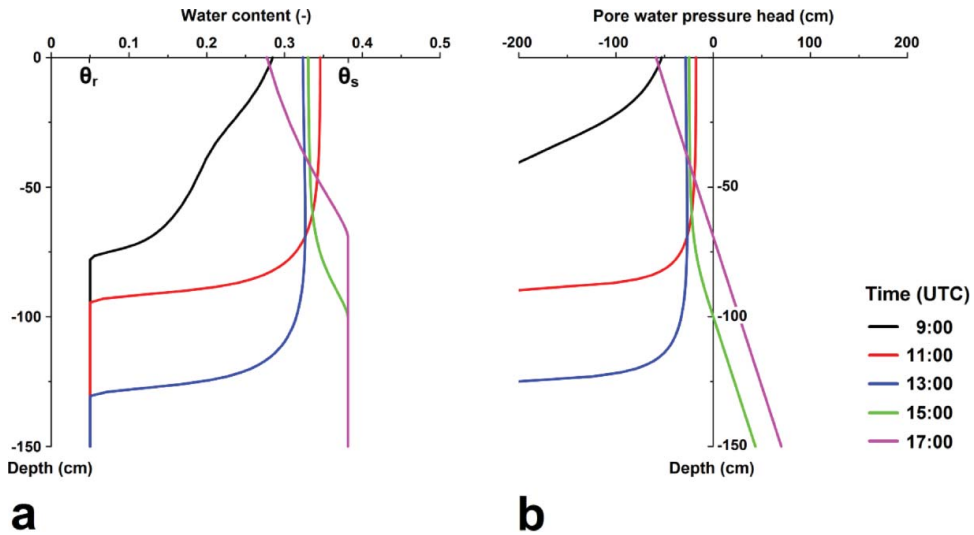


**Figure 15.** Water content (a) and pore water pressure trend (b) vs. depth, resulting from the HYDRUS 1D simulation of the 25th October 2011 rainfall event.

$\theta_r$ , but also  $\theta_s$  (saturated water content) and  $K_s$  (saturated hydraulic conductivity) on the basis of the soil grain size distribution by means of the ROSETTA Lite module (Schaap et al. 2001). As regards the grain-size data, we used the information from Cevasco et al. (2014) considering the above-mentioned similarities between the Monterosso and Vernazza basins.

According to the results of HYDRUS simulation, it was hypothesized the absence of an initial water table at the beginning of the 25th October 2011 event: thus, its depth ( $d_{wt}$ ) corresponds to the bedrock–soil interface. The  $I_{ZLT}$  parameter, that represents the long-term background rainfall rate, was assumed to be equal to the cumulative actual surface flux value, obtained by using the van Genuchten–Mualem model (van Genuchten 1980) for the simulation of the water flow. To evaluate  $\alpha_G$  parameter, that is typical of Gardner hydraulic model, we applied the conversion formula introduced by Ghezzehei et al. (2007) which defines a correspondence between Gardner and van Genuchten–Mualem models through the capillary length approach (Warrick 1995). However, in order to verify that the triggering of the landslides occurred during the 2011 event is actually related to an uprising of the perched water table (as assumed by TRIGRS), we extended the HYDRUS simulation also including the 25th October rainfall event. In this way, it was possible to describe the variation of water content (Figure 15(a)) and pore water pressure (Figure 15(b)) in response to the triggering rainfall. Starting from the initial soil moisture condition induced by the 1-month antecedent rainfall (black line in Figure 15(a)), the effect of such event results in a progressive increase of the water content within the unsaturated part of the soil, until reaching the complete saturation just in the lower portion between 13:00 and 15:00 UTC. At this point, a perched water table forms and progressively rises, up to a depth of approximately 70 cm at the end of the rainfall event. The same trend has been confirmed also for another extreme rainfall event occurred in the same area between 30 September and 4 October 1966 (see Section 2.2). However, it is important to note that in this case the initial soil moisture condition was wetter than that of the 2011 event, due to higher rainfall amounts prior to the event itself (Figure 16(a)): this point then explains how a similar final water table depth has been obtained from the simulation of the two events (Figure 16(b)), even though the 1966 rainfall event was less severe than the 2011 one (i.e. 263 vs 382 mm).

As regards the physical and mechanical properties of the colluvial deposits we again took into account the information from Cevasco et al. (2014). For the soil unit weight and friction angle we attributed an average value of  $16.33 \text{ kN/m}^3$  and  $31^\circ$ , respectively, considering the small variability of

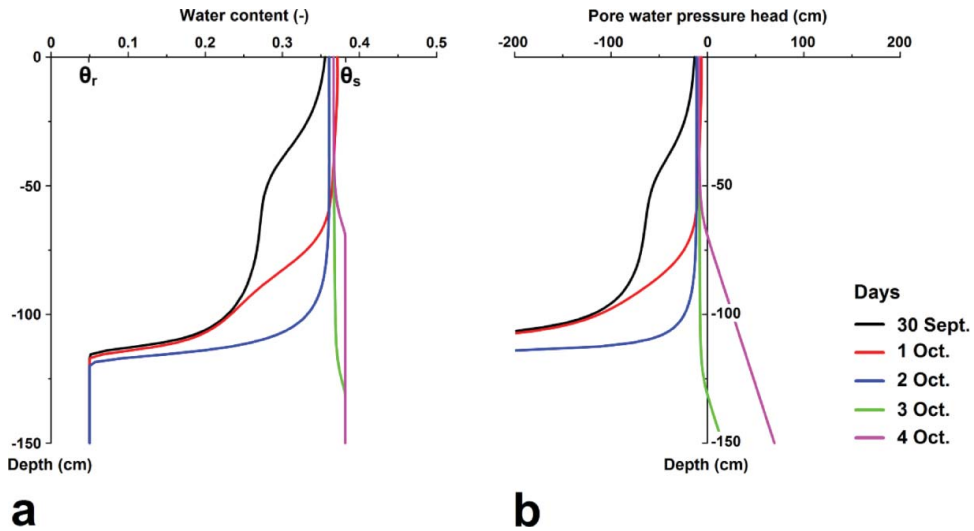


**Figure 16.** Water content (a) and pore water pressure trend (b) vs. depth, resulting from the HYDRUS 1D simulation of the 30th September–4th October 1966 rainfall event.

the values among the samples. On the contrary, we decided to calibrate the cohesion starting with an initial cautionary zero value, considering the high content of coarse grained particles within the eluvial–colluvial cover. Assuming that plant roots provide additional cohesion to the soil as a function of the vegetation type (e.g. Mickovski and van Beek 2009; Burylo et al. 2011), the calibration has been iterated until a minimum number of cells resulted as unstable before the beginning of the event. On the basis of the land-use map, the cohesion then varies between 4.5 kPa (in the case of recently abandoned terraces, where the vegetation is sparse) to 6 kPa, in correspondence of forest and scrubland areas (Table 2). However, it is important to note that the chosen values lie within the range of values reported by other authors for the same material (Mondini et al., 2009; Mazzuoli and Berardi 2016). At the same time, in the case of terraces that have been abandoned for a long time and forest/scrubland areas, we decided to attribute a value of saturated hydraulic conductivity up to one order of magnitude higher than that obtained through HYDRUS 1D simulations (i.e.  $4.63 \times 10^{-6} \text{ ms}^{-1}$ ), assuming that a much dense vegetation reduces the runoff, then favouring the seepage process. This assumption relies on the outcome of the comparative analysis between erosional processes and land use conducted by Cevasco et al. (2013a) in the Vernazza basin. In fact, the results of such analysis show that the land-use class most affected by runoff corresponds to the cultivated terraces: the frequency of such process progressively decreases passing from recently to long-time abandoned terraces, reaching its minimum in forest and scrubland areas. As a consequence, we attributed the following three different values of saturated hydraulic diffusivity:

$$D_0 = \frac{(K_s H)}{S_y} \quad (3)$$

where  $K_s$  is the saturated hydraulic conductivity,  $H$  is the average soil thickness (1.5 m) and  $S_y$  is the specific yield. If we consider that the investigated soil can be classified as sandy loam, the specific yield has been assumed equal to 0.29, on the basis of typical values given by Johnson (1967) for each soil textural class. Finally, with regard to the rainfall input during the landslide event, different hourly rainfall maps were made available by the Regional Environmental Agency (A.R.P.A.L. – Agenzia Regionale di Protezione dell'Ambiente Ligure). These

maps, which cover the entire event (i.e. 7-17 UTC), have been obtained by merging radar data and measurements from monitoring stations.

### 3.3. Statistical analysis of historical rainfall data

In order to evaluate the RP of landslide-triggering rainfall events, we performed a statistical analysis of maximum hourly rainfall intensity data. For this aim, we used data recorded by the Levanto monitoring station, that is the rain gauge closest to the study area for which this type of data is available for a long time span (i.e. between 1954 and 2012). The hydrological–statistical model is based on the analysis of the maximum values assumed by the chosen hydrological variable (i.e. cumulative rainfall at different hourly intervals). Specifically, we used the generalized extreme value (GEV) distribution (Jenkinson 1955), which is widely used in extreme event frequency analysis rather than the Gumbel distribution, as the literature increasingly suggests that the distribution of extreme events may be more heavily tailed (Fowler and Kilsby 2003). The cumulative distribution function of the GEV distribution is as follows:

$$F(x) = \exp \left\{ - \left( 1 + \zeta \frac{x - \mu}{\sigma} \right)^{1/\zeta} \right\} \quad (4)$$

where  $\mu$ ,  $\sigma$  and  $\zeta$  are referred to as the location, scale and shape parameters, respectively. These parameters have been determined by applying the probability weighted moment (PWM) method (Hosking et al. 1985), on the basis of the maximum values of each ‘cumulative rainfall’ variable (i.e. 1-, 3-, 6-, 12- and 24-h rainfall) extracted, year by year, from the dataset. Finally, the inversion of the probability function yields the values of cumulated rainfall  $x$  for each of the variables and for different RPs. Then, these values have been fitted by a power law distribution in order to build the rainfall probability curves.

## 4. Results

### 4.1. Back-analysis of the 25th October 2011 event

Once the input parameters of the numerical model have been defined, the 25th October 2011 event has been reproduced and the simulation results, expressed in terms of safety factor (FS), have been compared with the actual source areas of the landslides triggered during the event (Figure 17). In detail, we performed a ROC (Receiver Operating Characteristic) curve analysis in order to quantify the predictive performance of the numerical model. In fact, this type of analysis measures, for different thresholds (i.e. different values of FS), the proportion of positive values (i.e. landslide presence) that are correctly identified as such (TPR; True Positive Rate or sensitivity) together with the proportion of negative values (i.e. landslide absence) that are erroneously reported as positive (FPR; False Positive Rate or fall-out). The area under the curve (AUC) is the value that summarizes the expected performance: the larger the area, the better the accuracy of the model. According to the results (Table 5), the higher values of AUC have been obtained with the mean resolutions (2 and 4 m). It can be also noted that with the exception of the 1-m ones, the simulations which consider the spatial variation of the soil thickness based on the topographic position index (TPI) method are slightly better than those using the soil thickness resulting from the Saulnier's method (‘SAU’). In particular, the best AUC result corresponds to the TPI\_4-m simulation: for this reason, we analysed the temporal evolution of the instability with these conditions (Table 6). In this respect, calculating the relative percentage ( $P_U$ ) of predicted unstable pixels, it results that only 0.6% of pixels are indicated as unstable at 7:00 UTC (beginning of the rainfall event). After a small increase in the following 4 h, the instability rapidly rose after 11:00 UTC, progressively increasing until the end of the event. Therefore, almost all the landslides would have occurred in just 5 h, since the  $P_U$  passed from

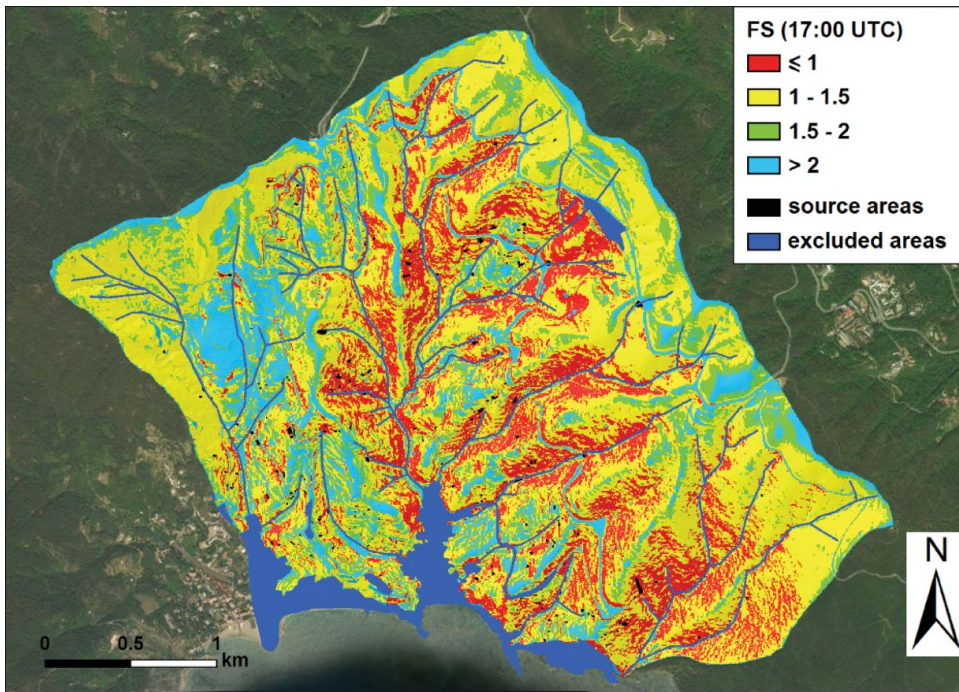


**Figure 17.** Graphical comparison between the spatial distribution of the 25th October 2011 landslide source areas (in black) and the slope stability conditions, expressed in terms of safety factor (FS), according to the TRIGRS model for the TPI\_4-m simulation.

**Table 5.** The AUC values deriving from the ROC analysis of the results of the numerical simulations.

<i>Simulation type</i>	<i>AUC</i>
TPI_1-m	66.5
SAU_1-m	71.5
TPI_2-m	73.0
SAU_2-m	72.9
TPI_4-m	74.8
SAU_4-m	72.4
TPI_8-m	71.0
SAU_8-m	70.5

**Table 6.** Number and relative percentage of pixels predicted as unstable ( $P_U$ ) by TRIGRS at different times during the 25th October 2011 event.

<i>Time (UTC)</i>	<i>No. of unstable cells</i>	<i><math>P_U</math> (%)</i>
7:00	372	0.6
8:00	2,742	4.4
9:00	2,789	4.5
10:00	3,157	5.1
11:00	4,254	6.8
12:00	6,952	11.1
13:00	12,826	20.6
14:00	22,566	36.2
15:00	40,651	65.1
16:00	62,402	100
17:00	62,402	100

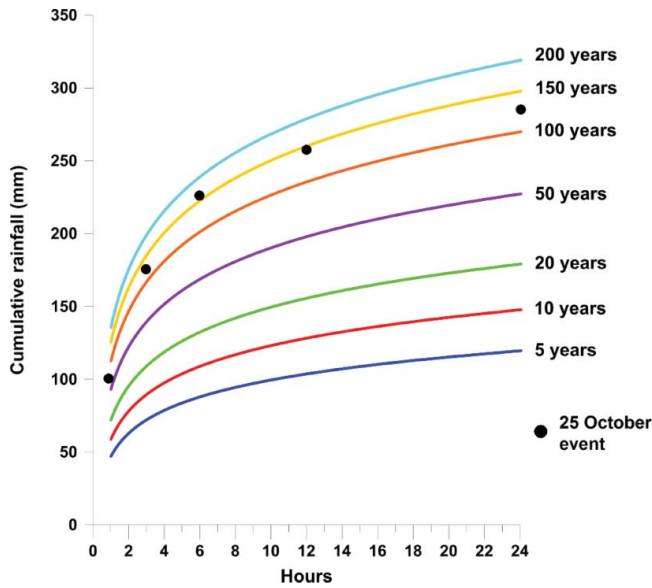


**Figure 18.** Rainfall probability curves for different return periods resulting from the historical data recorded at Levanto monitoring station. Black points indicate the maximum values of rainfall accumulated in 1, 3, 6, 12 and 24 h on 25 October 2011 (data from Regione Liguria 2012).

6.8% to 100% between 11:00 and 16:00 UTC, and the landslide event can be considered as concluded at 16:00 UTC, given the absence of further increases in slope instability after this time. It is worth noting how the final instability peak occurs in correspondence of the maximum rainfall peak, which took place approximately between 13:00 and 14:00 UTC (Figure 4).

#### 4.2. Evaluation of future triggering scenarios

After the back analysis of the 25th October 2011 event, we used the same model to predict the slope stability conditions of the study area by assuming different rainfall inputs, deriving from the statistical analysis of historical rainfall data described above. In this respect, the resulting rainfall probability curves (Figure 18) emphasize how the 2011 event can be classified as an exceptional event, considering the high RP calculated for each rainfall duration (Table 7). On the basis of these results, which confirm those obtained in a preceding analysis (A.R.P.A.L.-C.F.M.I.-P.C. 2011), three rainfall values corresponding to three different RPs (i.e. 25, 50 and 75 years) have been used, in order to evaluate the effect of more frequent rainfall events with respect to the 2011 one.

With regard to the other input parameters of the model, those used for the TPI-4 m simulation of the 2011 event have been kept: in this way, by assuming the same initial conditions it was possible to perform a straight comparison with the reference landslide event. Table 8 shows the importance, in

**Table 7.** Estimated return period (RP) for the maximum values of rainfall accumulated in 1, 3, 6, 12 and 24 h according to the data recorded at Levanto monitoring station during the 25th October 2011 event (rainfall data from Regione Liguria 2012).

Cumulated hours	25th October 2011 maximum rainfall (mm)	RP (years)
1	97.8	85
3	175.2	130
6	223.8	157
12	256.2	146
24	273.4	141



**Table 8.** Number of unstable pixels predicted by TRIGRS in response to the simulated rainfall scenario.

Rainfall duration	RP (years)	Rainfall amount (mm)	No. of unstable pixels	$P_{2011}$ (%)
1 h	25	72	4,175 (8)	6.7
	50	82	4,493 (8)	7.2
	75	89	4,715 (8)	7.6
3 h	25	121	8,882 (6)	14.2
	50	150	11,414 (6)	18.3
	75	169	13,487 (6)	21.6
6 h	25	144	20,524 (6)	32.9
	50	178	23,928 (6)	38.3
	75	201	27,681 (4)	44.4
12 h	25	167	31,414 (4)	50.3
	50	199	36,490 (4)	58.5
	75	220	39,878 (4)	63.9

Note: The parenthesized number indicates the delay (in hours) between the end of the rainfall event and the instability peak.

$P_{2011}$  represents the percentage of the maximum number of predicted unstable pixels compared to those obtained in the back-analysis of the 25th October 2011 event.

terms of produced instability, of the 6 and 12 h rainfall amount, also for a RP equal to 25 years. In this respect, the 12-h rainfall would cause about half (50.3%) of the slope instability calculated for the entire 25th October 2011 event. In the case of 6 h rainfall, a similar level of instability develops only for events with RP equal to 75 years. On the contrary, for rainfall events having shorter duration (1 and 3 h), the number of unstable pixels is quite low even considering high RPs. However, in each rainfall condition it can be noted a certain delay between the end of the rainfall event and the instability peak: in fact, the maximum number of unstable pixels can be observed 4–8 h later, depending on the rainfall length (i.e. the less the duration, the greater the delay). This point can be explained considering the time needed for water to reach the greater soil depths, and this delay is greater for short rainfall events, considering the reduced duration of the seepage process during the event itself.

## 5. Discussions

The back-analysis performed by using TRIGRS emphasizes that the 2-m and 4-m DEMs are the most suitable for the reconstruction of the 2011 landslide event, as they yield the highest AUC values. In fact, if we compare the TPR, the FPR and the accuracy (i.e. the ratio between the total number of correct predictions and the total number of observations) obtained, for each performed simulation, by imposing a threshold FS value equal to 1 (Table 9), it can be noted that:

- (1) The SAU\_1-m simulation is able to predict the 2011 landslide occurrence significantly better than the corresponding TPI simulation, given the highest TPR. However, the resulting accuracy (73.8%) is lower than those obtained from the 2-m and 4-m simulations due to the higher FPR. All these false alarms can be explained considering that the high resolution

**Table 9.** True positive rate (TPR), false positive rate (FPR) and accuracy values resulting from the comparison between the FS maps obtained with TRIGRS and the 2011 landslide source areas.

Simulation type	TPR	FPR	ACCURACY
TPI_1-m	45.7	18.3	81.6
SAU_1-m	57.9	26.1	73.8
TPI_2-m	54.4	19.5	80.4
SAU_2-m	57.2	24.5	75.4
TPI_4-m	49.5	18.2	81.7
SAU_4-m	48.9	22.1	77.8
TPI_8-m	35.8	12.4	87.4
SAU_8-m	39.7	19.3	80.5

implies an extreme heterogeneity of the local slope which, in turn, determines an undue spatial variation of the soil thickness, which then influences the model output (Figure 19);

- (2) The TPI\_2-m and 4-m simulations show higher accuracy values compared to the corresponding SAU simulations because the number of false alarms is lower, even though the TPR values are similar. As regards the TPI simulations, it can be also noted that the 2-m simulation correctly identifies the landslide source areas slightly better than the 4-m one, and vice versa. However, as stated above, the best result in terms of AUC has been obtained

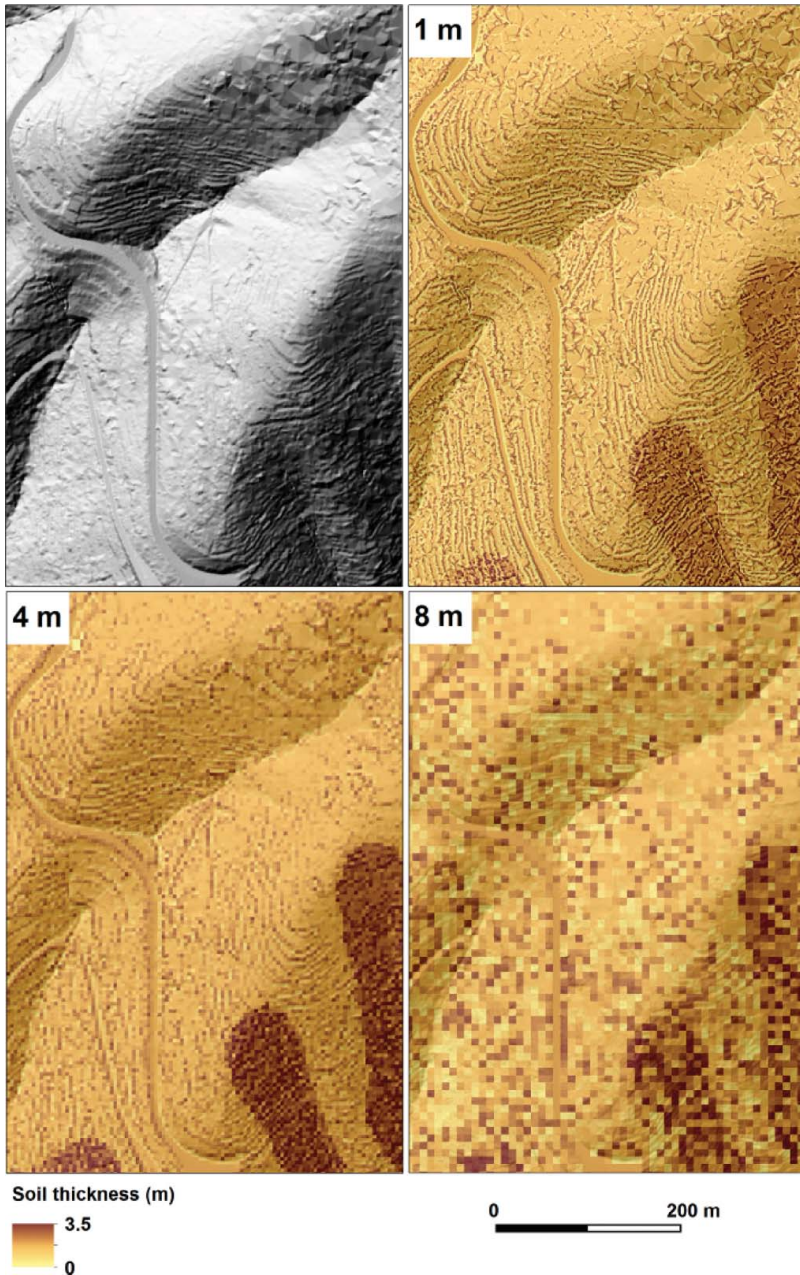


Figure 19. Graphical comparison between the hillshade of the 1-m DEM (upper left) and the 1-m, 4-m and 8-m soil thickness maps, obtained by means of the Topographic Position Index method.

**Table 10.** True positive rate (TPR), false positive rate (FPR) and accuracy values resulting from the comparison between the 4-m FS maps obtained with TRIGRS and the 2011 landslide source areas. The analyses have been performed by distinguishing terraced and not-terraced areas.

<i>Simulation type</i>	<i>TPR</i>	<i>FPR</i>	<i>ACCURACY</i>
TPI_4-m terraced areas	50.7	25.7	74.2
SAU_4-m terraced areas	50.0	31.1	68.8
SAU_4-m not-terraced areas	17.2	0.8	99.2

with the TPI\_4-m simulation: this means that this spatial resolution, coupled with the TPI method, allows to efficiently reproduce the shallow slope failures by keeping the spatial information concerning the pattern of the agricultural terraces (Figure 19). In this respect, for this spatial resolution we also calculated the TPR, FPR and accuracy by distinguishing between terraced and not terraced areas (Table 10). As it can be noticed, the use of TPI method allows to increase the accuracy in the terraced areas of more than 5 percentage points due to the reduction of FP. With regard to the not-terraced areas, although the TPR is very low, the accuracy is extremely high since just very few source areas are located in such areas;

- (3) The TPI and SAU\_8-m simulations tend to underestimate the landslide occurrence, according to the low TPR. This result can be explained considering that the coarseness of the spatial resolution makes it difficult to properly reproduce either the shape of the landslide source areas or the real pattern of the agricultural terraces, unlike the highest resolutions (Figure 19).

At this point, considering that the best results have been obtained with the 2-m and 4-m resolutions, we performed a further analysis to quantify the number of simulated landslides to changing the percentage of correctly predicted source area. In other words, assuming that a landslide can be considered ‘triggered’ if at least 50%, 60%,...,100% of pixels within the source area polygon results as ‘unstable’, we calculated the percentage of landslides properly computed with the two spatial resolutions and considering the two different methods for the estimation of the soil thickness (Figure 20). The results show that the 2-m simulations identify a slightly higher number of landslides compared to the 4-m simulations, but only for low thresholds of correctly predicted source area (50%–60%). In fact, a rapid reduction of the number of correctly simulated landslides can be noted with increasing the percentage of correctly predicted source area. On the contrary, the reduction is much less pronounced in the case of the 4-m simulations, which show a relatively high percentage of correctly simulated landslides even for high thresholds. In addition, the comparison between TPI and SAU simulations indicates that for the 2-m simulations the best results have been obtained with the Saulnier’s method, unlike the 4-m simulations. This point confirms how the TPI method is the most

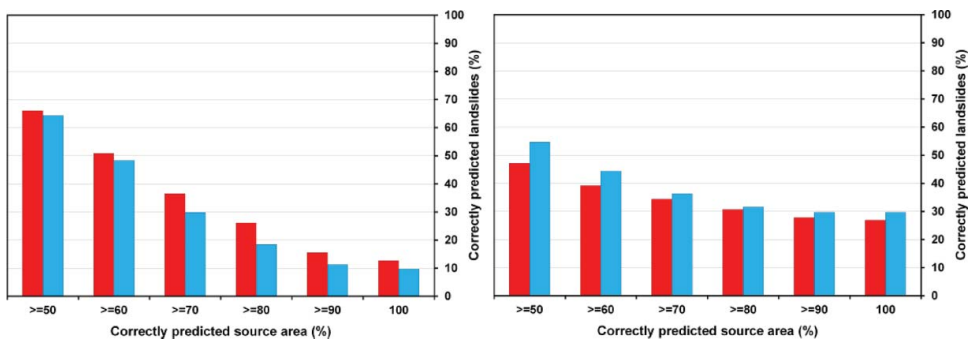


**Figure 20.** Percentage of correctly simulated landslides to changing the percentage of correctly predicted source area according to 2-m (left) and 4-m (right) numerical simulations. The red and blue bars refer to the SAU and TPI simulations, respectively.

suitable technique for the estimation of the spatial variation of the soil thickness, at least considering the topographic peculiarities of the Cinque Terre area.

As far as the evaluation of future triggering scenarios is concerned, the results show that the highest amounts of unstable pixels have been obtained for the longest rainfall events (i.e. 6–12 h). In fact, considering the relatively low hydraulic conductivity of the soil together with the unsaturated conditions, the partial absorption of water infiltrating at the surface results in damping and smoothing of the rainfall input, which cause the triggering of fairly few cells in response to short rainfall events. In this respect, if we compare these results with those obtained for the case study occurred in Giampieri in 2009 (see Section 3.2), it can be noted that – in that instance – the wetter initial soil moisture conditions resulted in a high number of unstable cells even in response to short rainfall events (Schilirò et al. 2015a). From this point of view those initial soil moisture conditions have certainly enhanced the triggering of shallow landslides, also considering that the 2009 rainfall event was far from exceptional, at least if compared with that occurred in the Monterosso catchment in 2011. This finding then emphasizes that, within the definition of realistic triggering scenarios for rainfall-induced shallow landslides, it is essential a proper evaluation not only of the expected rainfall event but also of the soil hydraulic properties and the initial moisture conditions.

## 6. Conclusions

In this study, we used a physically based model for the prediction of rainfall-induced shallow landslides in a coastal catchment located in the Cinque Terre area (Eastern Liguria, Northern Italy). As a first step, we performed a back-analysis of a landslide event occurred in the study area on 25 October 2011 by using four different spatial resolutions of the digital terrain model and two different methods for the evaluation of the spatial variation of the soil thickness. The results indicate that the numerical simulations reconstruct quite well the space-time evolution of the real event and, more specifically, that the best results have been obtained with the mean resolutions (2 and 4 meters) and considering the TPI method as the technique for the spatial definition of the soil thickness. In particular, the best result in terms of AUC has been obtained with the TPI\_4-m simulation, which confirms that the spatial information concerning the pattern of the agricultural terraces is maintained even at this resolution. At a broader level, it can be also asserted that the TPI method is slightly better than the SAU method since it allows to reduce the false alarms (FP) without reducing the number of correctly predicted landslide pixels (TP). With regard to the evaluation of the RP of the 2011 event, the results confirm the exceptionality of the event itself. However, the analysis of different triggering scenarios shows that long (6–12 h) rainfall events even with relatively low RP can cause a substantial instability level: this latter point would therefore explain the landslide/flood events that have occurred in the past in the same area. The results of the numerical simulations also emphasize the importance of the specific local conditions (such as, in this case, the widespread presence of agricultural terraces) in influencing the occurrence of shallow landslides. For the parameterization of the numerical model we have then considered that different land-use types affect not only the spatial distribution of the soil thickness, but also the geotechnical parameters and the hydraulic conditions of the soil: in our opinion, these aspects cannot be disregarded in this type of analysis and, if taken into account, allow to obtain reliable results. Although future improvements will definitely concern a better evaluation of the input parameters, from a methodological point of view we believe that the proposed approach enhances the potential of physically based models as tools for hazard assessment and risk management.


## Acknowledgements

The authors thank an anonymous referee for his/her helpful suggestions and constructive comments, which have contributed greatly in improving the quality of the manuscript. The authors also thank Massimo Pecci from “Dipartimento per gli Affari Regionali e le Autonomie della Presidenza del Consiglio dei Ministri” for his technical and logistic support.

## Disclosure statement

No potential conflict of interest was reported by the authors.

## ORCID

Luca Schilirò  <http://orcid.org/0000-0002-6461-2802>

## References

- Abbate E. 1969. Geologia delle Cinque Terre e dell'entroterra di Levante (Liguria orientale). *Memorie della Società Geologica Italiana*. 8:923–1014.
- Aleotti P, Chowdhury R. 1999. Landslide hazard assessment: summary review and new perspectives. *Bull Eng Geol Environ*. 58:21–44. doi: 10.1007/s100640050066.
- A.R.P.A.L.-C.F.M.I.-P.C. (Agenzia Regionale per la Protezione dell'Ambiente Ligure-Centro Funzionale Meteorologico di Protezione Civile della Regione Liguria). 2011. Alluvioni in Liguria, i fattori meteo e gli effetti. *Ecoscienza*. 5:6–9.
- Baeza C, Corominas J. 2001. Assessment of shallow landslide susceptibility by means of multivariate statistical techniques. *Earth Surf Proc Land*. 26:1251–1263. doi: 10.1002/esp.263.
- Baum RL, Godt JW, Savage WZ. 2010. Estimating the timing and location of shallow rainfall-induced landslides using a model for transient, unsaturated infiltration. *J Geophys Res*. 115:F03013. doi: 10.1029/2009JF001321.
- Baum RL, Savage WZ, Godt JW. 2008. TRIGRS – A Fortran program for transient rainfall infiltration and grid-based regional slope-stability analysis, version 2.0. Reston (VA): U.S. Geological Survey. Report No.: 2008-115 9.
- Begueria S. 2006. Changes in land cover and shallow landslide activity: a case study in the Spanish Pyrenees. *Geomorphology*. 74:196–206. doi: 10.1016/j.geomorph.2005.07.018.
- Borga M, Dalla Fontana G, Gregoretti C, Marchi L. 2002. Assessment of shallow landsliding by using a physically based model of hillslope stability. *Hydrol Process*. 16:2833–2851. doi: 10.1002/hyp.1074.
- Borja RI, Liu X, White JA. 2012. Multiphysics hillslope processes triggering landslides. *Acta Geotechnica*. 7:261–269. doi: 10.1007/s11440-012-0175-6.
- Brandolini P, Cevasco A, Capolongo D, Pepe G, Lovergine F, Del Monte M. 2016. Response of terraced slopes to a very intense rainfall event and relationships with land abandonment: a case study from Cinque Terre (Italy). *Land Degrad Dev*. [Accessed 2017 November 24]: [13 p.]. doi: 10.1002/ldr.2672.
- Burylo M, Hudek C, Rey F. 2011. Soil reinforcement by the roots of six dominant species on eroded mountainous marly slopes (Southern Alps, France). *Catena*. 84:70–78. doi: 10.1016/j.catena.2010.09.007.
- Buzzi, A, Davolio S, Malguzzi P, Drofa O, Mastrangelo D. 2014. Heavy rainfall episodes over Liguria of autumn 2011: numerical forecasting experiments. *Nat Hazards Earth Syst Sci*. 14:1325–1340. doi:10.5194/nhess-14-1325-2014.
- Carrara A. 1983. Multivariate models for landslide hazard evaluation. *Math Geol*. 15:403–426. doi: 10.1007/BF01031290.
- Carrara A, Crosta G, Frattini P. 2008. Comparing models of debris-flow susceptibility in the alpine environment. *Geomorphology*. 94:353–378. doi: 10.1016/j.geomorph.2006.10.033.
- Casadei M, Dietrich WE, Miller L. 2003. Testing a model for predicting the timing and location of shallow landslide initiation in soil-mantled landscapes. *Earth Surf Proc Land*. 28:925–950. doi: 10.1002/esp.470.
- Castro Camilo D, Lombardo L, Martin Mai P, Dou J, Huser R. 2017. Handling high predictor dimensionality in slope-unit-based landslide susceptibility models through LASSO-penalized Generalized Linear Model. *Environ Model Soft*. 97:145–156. doi: 10.1016/j.envsoft.2017.08.003.
- Cassola F, Ferrari F, Mazzino A, Miglietta MM. 2016. The role of the sea on the flash floods events over Liguria (northwestern Italy). *Geophys Res Lett*. 43:3534–3542. doi: 10.1002/2016GL068265.
- Catani F, Segoni S, Falorni G. 2010. An empirical geomorphology-based approach to the spatial prediction of soil thickness at catchment scale. *Water Resour Res*. 46:W05508. doi: 10.1029/2008WR007450.
- Cevasco A, Brandolini P, Scopesi C, Rellini I. 2013a. Relationships between geo-hydrological processes induced by heavy rainfall and land-use: the case of 25 October 2011 in the Vernazza catchment (Cinque Terre, NW Italy). *J Maps*. 9:289–298. doi: 10.1080/17445647.2013.780188.
- Cevasco A, Diodato N, Revellino P, Fiorillo F, Grelle G, Guadagno FM. 2015. Storminess and geohydrological events affecting small coastal basins in a terraced Mediterranean environment. *Sci Total Environ*. 532:208–219. doi: 10.1016/j.scitotenv.2015.06.017.
- Cevasco A, Francioli G, Robbiano A, Sacchini A, Vincenzi E. 2009. Methodological procedures for landslide's risk mitigation for civil protection purposes in the Genoa municipality area. *Rendiconti Online Società Geologica Italiana*. 6:152–153.



- Cevasco A, Pepe G, Brandolini P. 2012. Shallow landslides induced by heavy rainfall on terraced slopes: the case study of the October, 25, 2011 event in the Vernazza catchment (Cinque Terre, NW Italy). *Rendiconti Online Società Geologica Italiana*. 21:384–386.
- Cevasco A, Pepe G, Brandolini P. 2013b. Geotechnical and stratigraphic aspects of shallow landslides at Cinque Terre (Liguria, Italy). *Rendiconti Online Società Geologica Italiana*. 24:52–54.
- Cevasco A, Pepe G, Brandolini P. 2014. The influences of geological and land use settings on shallow landslides triggered by an intense rainfall event in a coastal terraced environment. *Bull Eng Geol Environ*. 73:859–875. doi: 10.1007/s10064-013-0544-x.
- Chang K, Chiang S, Feng L. 2008. Analysing the relationship between typhoon-triggered landslides and critical rainfall conditions. *Earth Surf Proc Land*. 33:1261–1271. doi: 10.1002/esp.1611.
- Chang K, Chiang S. 2009. An integrated model for predicting rainfall-induced landslides. *Geomorphology*. 105:366–373. doi: 10.1016/j.geomorph.2008.10.012.
- Crosta G. 1998. Regionalization of rainfall thresholds: an aid to landslide hazard evaluation. *Environ Geol*. 35:131–145. doi:10.1007/s002540050300.
- Cruden DM, Varnes DJ. 1996. Landslide types and processes. In: Turner AK, Schuster RL, editors. *Landslides investigation and mitigation*. Board Special Report. Vol. 247. Washington (DC): Transportation Research, US National Research Council; p. 36–75.
- D'Amato Avanzi G, Galanti Y, Giannecchini R, Bartelletti C. 2015. Shallow landslides triggered by the 25 October 2011 extreme rainfall in eastern Liguria (Italy). In: Lollino G, Giordan D, Crosta GB, Corominas J, Azzam R, Wasowski J, Sciarra N, editors. *Engineering geology for society and territory – Vol. 2*. Basel (Switzerland): Springer International Publishing; p. 515–519. doi: 10.1007/978-3-319-09057-3\_85.
- D'Amato Avanzi G, Galanti Y, Giannecchini R, Mazzali A, Saule G. 2013. Remarks on the 25 October 2011 rainstorm in Eastern Liguria and Northwestern Tuscany (Italy) and the related landslides. *Rendiconti Online Società Geologica Italiana*. 24:76–78.
- Dai FC, Lee CF, Ngai YY. 2002. Landslide risk assessment and management and management – an overview. *Eng Geol*. 64:65–87. doi: 10.1016/S0013-7952(01)00093-X.
- Ermini L, Catani F, Casagli N. 2005. Artificial Neural Networks applied to landslide susceptibility assessment. *Geomorphology*. 66:327–343. doi: 10.1016/j.geomorph.2004.09.025.
- Formetta G, Rago V, Capparelli G, Rigon R, Muto F, Versace P. 2014. Integrated physically based system for modeling landslide susceptibility. *Procedia Earth and Planetary Science*. 9:74–82. doi: 10.1016/j.proeps.2014.06.006.
- Fowler HJ, Kilsby CG. 2003. A regional frequency analysis of United Kingdom extreme rainfall from 1961 to 2000. *Int J Climatol*. 23:1313–1334. doi: 10.1002/joc.943.
- Galve JP, Cevasco A, Brandolini P, Soldati M. 2015. Assessment of shallow landslide risk mitigation measures based on land use planning through probabilistic modelling. *Landslides*. 12:101–114. doi: 10.1007/s10346-014-0478-9.
- Gardner WR. 1958. Some steady-state solutions of the unsaturated moisture flow equation with application to evaporation from a water table. *Soil Sci*. 85:228–232. doi: 10.1097/00010694-195804000-00006.
- Ghezzehei TA, Kneafsey TJ, Su GW. 2007. Correspondence of the Gardner and van Genuchten-Mualem relative permeability function parameters. *Water Resour Res*. 43:W10417. doi: 10.1029/2006WR005339.
- Glade T. 2003. Landslide occurrence as a response to land use change: a review of evidence from New Zealand. *Catena*. 51:297–314. doi: 10.1016/S0341-8162(02)00170-4.
- Goetz JN, Brenning A, Petschko H, Leopold P. 2015. Evaluating machine learning and statistical prediction techniques for landslide susceptibility modelling. *Computers and Geosciences*. 81:1–11. doi: 10.1016/j.cageo.2015.04.007.
- Goetz JN, Guthrie RH, Brenning A. 2011. Integrating physical and empirical landslide susceptibility models using generalized additive models. *Geomorphology*. 129:376–386. doi: 10.1016/j.geomorph.2011.03.001.
- Greco R, Guida A, Damiano E, Olivares L. 2010. Soil water content and suction monitoring in model slopes for shallow flowslides early warning applications. *Phys Chem Earth*. 35:127–136. doi: 10.1016/j.pce.2009.12.003.
- Guzzetti F, Cardinali M, Reichenbach P. 1994. The AVI Project: a bibliographical and archive inventory of landslides and floods in Italy. *Environ Manag*. 18:623–633. doi: 10.1007/BF02400865.
- Guzzetti F, Tonelli G. 2004. Information system on hydrological and geomorphological catastrophes in Italy (SICI): a tool for managing landslide and flood hazards. *Nat Hazards Earth Sys Sci*. 4:213–232. doi: 10.5194/nhess-4-213-2004.
- Ho JY, Lee KT. 2016. Performance evaluation of a physically based model for shallow landslide prediction. *Landslides*. 14:961–980. doi: 10.1007/s10346-016-0762-y.
- Hosking JRM, Wallis JR, Wood EF. 1985. Estimation of the generalized extreme value distribution by the method of probability weighted moments. *Technometrics*. 27:251–261. doi:10.1080/00401706.1985.10488049.
- Hungr O, Leroueil S, Picarelli L. 2014. The Varnes classification of landslide types, an update. *Landslides*. 11:167–194. doi: 10.1007/s10346-013-0436-y.
- Iverson RM. 2000. Landslide triggering by rain infiltration. *Water Resour Res*. 36:1897–1910. doi: 10.1029/2000WR900090.
- Jenkinson AF. 1955. The frequency distribution of the annual maximum (or minimum) values of meteorological events. *Q J R Meteorol Soc*. 87:158–171. doi:10.1002/qj.49708134804.

- Jensen DT, Hargreaves GH, Temesgen B, Allen RG. 1997. Computation of ETo under nonideal conditions. *J Irrig Drain E-Asce*. 123:394–400. doi: 10.1061/(ASCE)0733-9437(1997)123:5(394).
- Johnson AI. 1967. Specific yield-compilation of specific yields for various materials. Washington (DC): United States Government Printing Office. U.S. Geological Survey Water Supply Paper No. :1662-D.
- La Stampa (Turin, Italy) 1966. Monterosso e Levanto ancora invase dal fango. L'acqua è razionata, manca la luce elettrica. 1966 Oct 5 :10 (col. 2).
- Lee S. 2005. Application of logistic regression model and its validation for landslide susceptibility mapping using GIS and remote sensing data. *Int J Remote Sens*. 26:1477–1491. doi:10.1080/01431160412331331012.
- Lee S, Ryu J-H, Won J-S, Park H-J. 2004. Determination and application of the weights for landslide susceptibility mapping using an artificial neural network. *Eng Geol*. 71:289–302. doi: 10.1016/S0013-7952(03)00142-X.
- Li C, Ma T, Zhu X, Li W. 2011. The power-law relationship between landslide occurrence and rainfall level. *Geomorphology*. 130:221–229. doi: 10.1016/j.geomorph.2011.03.018.
- Liao Z, Hong Y, Kirschbaum D, Liu C. 2011. Assessment of shallow landslides from Hurricane Mitch in central America using a physically based model. *Environ Earth Sci*. 66:1697–1705. doi: 10.1007/s12665-011-0997-9.
- Lin CW, Liu SH, Lee SY, Liu CC. 2006. Impacts of the Chi-Chi earthquake on subsequent rainfall-induced landslides in central Taiwan. *Eng Geol*. 86:87–101. doi: 10.1016/j.enggeo.2006.02.010.
- Marjanović M, Kovačević M, Bajat B, Voženilek V. 2011. Landslide susceptibility assessment using SVM machine learning algorithm. *Engineering Geology*. 123:225–234. doi: 10.1016/j.enggeo.2011.09.006.
- Mazzuoli M, Berardi R. 2016. Numerical simulation of a debris flow propagation: a case of study in the Cinque Terre, Liguria. In: Aversa S, Cascini L, Picarelli L, Scavia C, editors. *Landslides and engineered slopes. Experience, theory and practice: Proceedings of the 12th International Symposium on Landslides; 12–19 June 2016; Naples (Italy)*. Leiden (The Netherlands): CRC Press/Balkema. p. 1393–1400.
- Mickovski SB, van Beek LPH. 2009. Root morphology and effects on soil reinforcement and slope stability of young vetiver (*Vetiveria zizanioides*) plants grown in semi-arid climate. *Plant and Soil*. 324:43–56. doi: 10.1007/s11104-009-0130-y.
- Mondini AC, Viero A, Cavalli M, Marchi L, Herrera G, Guzzetti F. 2009. Comparison of event landslide inventories: the Pogliaschina catchment test case, Italy. *Nat Hazards Earth Syst Sci*. 14:1749–1759. doi: 10.5194/nhess-14-1749-2014.
- Montgomery DR, Dietrich WE. 1994. A physically based model for the topographic control on shallow landsliding. *Water Resour Res*. 30:1153–1171. doi: 10.1029/93WR02979.
- Montrasio L. 2000. Stability analysis of soil slip. In: Brebbia CA, editors. *Proceedings of International Conference "Risk 2000"*. Southampton: Wit Press; p. 357–366.
- Montrasio L, Schilirò L, Terrone A. 2016. Physical and numerical modelling of shallow landslides. *Landslides*. 13:873–883. doi: 10.1007/s10346-015-0642-x.
- Montrasio L, Valentino R. 2007. Experimental analysis and modelling of shallow landslides. *Landslides*. 4:291–296. doi: 10.1007/s10346-007-0082-3.
- Montrasio L, Valentino R. 2008. A model for triggering mechanisms of shallow landslides. *Nat Hazards Earth Syst Sci*. 8:1149–1159. doi: 10.5194/nhess-8-1149-2008.
- Pedemonte R. 2005. Contributo alla classificazione dei climi della Liguria – distribuzione geografica delle precipitazioni annue, IV parte. *Rivista Ligure di Meteorologia*. [accessed 2017 Apr 13]:[4 p.]. [http://www.nimbus.it/liguria/rlm14/climatologia/clima\\_liguria/stampa\\_clima\\_liguria.pdf](http://www.nimbus.it/liguria/rlm14/climatologia/clima_liguria/stampa_clima_liguria.pdf)
- Persichillo MG, Bordoni M, Meisina C, Bartelletti C, Barsanti M, Giannecchini R, D'Amato Avanzi G, Galanti Y, Cevasco A, Brandolini P, et al. 2016. Shallow landslides susceptibility assessment in different environments. *Geomat Nat Hazards Risk*. 8:748–771. doi: 10.1080/19475705.2016.1265011.
- Pham BT, Bui DT, Prakash I, Dholakia MB. 2017. Hybrid integration of Multilayer Perceptron Neural Networks and machine learning ensembles for landslide susceptibility assessment at Himalayan area (India) using GIS. *Catena*. 149:52–63. doi: 10.1016/j.catena.2016.09.007.
- Piacentini D, Troiani F, Soldati M, Notarnicola C, Savelli D, Schneiderbauer S, Strada C. 2012. Statistical analysis for assessing shallow-landslide susceptibility in South Tyrol (south-eastern Alps, Italy). *Geomorphology*. 151-152:196–206. doi: 10.1016/j.geomorph.2012.02.003.
- Rebora N, Molini L, Casella E, Comellas A, Fiori E, Pignone F, Siccardi F, Silvestro F, Tanelli S, Parodi A. 2013. Extreme rainfall in the Mediterranean: What can we learn from observations? *J Hydrometeorol*. 14:906–922. doi: 10.1175/JHM-D-12-083.1.
- Regione Liguria. 2005. Carta geologica – La Spezia – Tavoleta no. 248.4 (scala 1:25,000) [geological map]. Florence (Italy): S.EL.CA. society.
- Regione Liguria. 2012. *Ambiente in Liguria – catalogo banche dati*[database]. Genova (Italy): Regione Liguria. [updated 2017 May 4; accessed 2017 May 4]. <http://www.banchedati.ambienteinliguria.it/index.php/aria/meteo>.
- Saulnier GM, Beven K, Obled C. 1997. Including spatially variable effective soil depths in TOPMODEL. *J Hydrol*. 202:158–172. doi: 10.1016/S0022-1694(97)00059-0.
- Savage WZ, Godt JW, Baum RL. 2003. A model for spatially and temporally distributed shallow landslide initiation by rainfall infiltration. In: Rickenmann D, Chen CL, editors. *Debris-flow hazards mitigation: mechanics, prediction and assessment*. Rotterdam: Millpress; p. 179–187.

- Schaap MG, Leij FJ, van Genuchten MTh. 2001. ROSETTA: a computer program for estimating soil hydraulic parameters with hierarchical pedotransfer functions. *J Hydrol.* 251:163–176. doi: 10.1016/S0022-1694(01)00466-8.
- Schilirò L, De Blasio FV, Esposito C, Scarascia Mugnozza G. 2015b. Reconstruction of a destructive debris-flow event via numerical modelling: the role of valley geometry on flow dynamics. *Earth Surf Proc Land.* 40:1847–1861. doi: 10.1002/esp.3762.
- Schilirò L, Esposito C. 2013. Susceptibility assessment and triggering scenarios for shallow landslides in the southern Messina province (north-eastern Sicily, Italy) using statistic-probabilistic and deterministic approaches. *Rendiconti Online Società Geologica Italiana.* 24:298–300.
- Schilirò L, Esposito C, Scarascia Mugnozza G. 2015a. Evaluation of shallow landslide-triggering scenarios through a physically based approach: an example of application in the southern Messina area (northeastern Sicily, Italy). *Nat Hazards Earth Syst Sci.* 15:2091–2109. doi: 10.5194/nhess-15-2091-2015.
- Schilirò L, Montrasio L, Scarascia Mugnozza G. 2016. Prediction of shallow landslide occurrence: validation of a physically-based approach through a real case study. *Sci Total Environ.* 569–570:134–144. doi: 10.1016/j.scitotenv.2016.06.124.
- Silvestro F, Gabellani S, Giannoni F, Parodi A, Rebora N, Rudari R, Siccardi F. 2012. A hydrological analysis of the 4 November 2011 event in Genoa. *Nat Hazards Earth Syst Sci.* 12:2743–2752. doi:10.5194/nhess-12-2743-2012.
- Silvestro F, Rebora N, Giannoni F, Cavallo A, Ferraris L. 2015. The flash flood of the Bisagno Creek on 9th October 2014: an unfortunate combination of spatial and temporal scales. *J Hydrol.* 541:50–62. doi: 10.1016/j.jhydrol.2015.08.004.
- Šimůnek J, Huang M, Šejna M, van Genuchten MTh. 1998. The HYDRUS-1D software package for simulating the one-dimensional movement of water, heat, and multiple solutes in variably-saturated media – Version 1.0. International Ground Water Modeling Center. Golden (CO): Colorado School of Mines; p. 186 p.
- Soeters R, Van Westen CJ. 1996. Slope instability recognition, analysis and zonation. In: Turner AK, Schuster RL, editors. *Landslides investigation and mitigation.* Vol. 247. Washington (DC): Transportation Research, US National Research Council. Board Special Report; p. 129–177.
- Thierry Y, Vandromme R, Maquaire O, Bernardie S. 2017. Landslide susceptibility assessment by EPBM (Expert Physically Based Model): strategy of calibration in complex environment. In: Mikoš M, Arbanas Ž, Yin Y, Sassa K, editors. *Advancing culture of living with landslides.* 4th World Landslide Forum; 29th May – 2nd June; Ljubljana, 2017, p. 917–926.
- Trigila A, Iadanza C, Esposito C, Scarascia Mugnozza G. 2015. Comparison of Logistic Regression and Random Forests techniques for shallow landslide susceptibility assessment in Giampilieri (NE Sicily, Italy). *Geomorphology.* 249:119–136. doi: 10.1016/j.geomorph.2015.06.001, 2015.
- van Delden A. 2001. The synoptic setting of thunderstorms in Western Europe. *Atmos Res.* 56:89–110. doi: 10.1016/S0169-8095(00)00092-2.
- van Genuchten MTh. 1980. A closed-form equation for predicting the hydraulic conductivity of unsaturated soils. *Soil Sci Soc Am J.* 44:892–898. doi: 10.2136/sssaj1980.03615995004400050002x.
- Warrick AW. 1995. Correspondence of hydraulic functions for unsaturated soils. *Soil Sci Soc Am J.* 59:292–299. doi: 10.2136/sssaj1995.03615995005900020003x.
- Weiss A. 2001. Topographic position and landforms analysis. Poster session presented at ESRI User Conference; San Diego (CA). Available from: [http://www.jennessent.com/downloads/tpi-poster-tnc\\_18x22.pdf](http://www.jennessent.com/downloads/tpi-poster-tnc_18x22.pdf).
- Youssef AM, Pourghasemi HR, Pourtaghi ZS, Al-Katheeri MM. 2016. Landslide susceptibility mapping using random forest, boosted regression tree, classification and regression tree, and general linear models and comparison of their performance at Wadi Tayyah Basin, Asir Region, Saudi Arabia. *Landslides.* 13:839–856. doi: 10.1007/s10346-015-0614-1.
- Zhang H, Zhang WW. 2009. Rainfall infiltration in cracked soil and its effect on slope stability analysis. In: Buzzi O, Fityus S, Sheng D, editors. *Unsaturated Soils: Proceedings of the 4th Asia Pacific Conference on Unsaturated Soils.* Newcastle: CRC Press; p. 313–318, ISBN: 9780415804806.